

Dear Dr. Laskin,

Below we provide a point-by-point response to the reviewers' comments and a track-changes version of our revised manuscript. We have made extensive revisions, with a particular eye towards properly expressing uncertainties, that we believe have fully addressed the reviewers comments. Please let us know if you have any questions.

Regards,

Chris Cappa (UC Davis) and Dean Atkinson (Portland State University)

We thank the reviewers for their careful reading of the manuscript and their comments and suggestions. We have addressed each of their queries and believe that the paper is strengthened. Our point-by-point responses to the Reviewers' comments and suggestions follow below.

The reviewer comments are in black and our responses in blue. New text added to the manuscript is *italicized*.

## Reviewer #2

### Summary and General Comments

The work presented by Atkinson *et al.* applies a spectral deconvolution algorithm (SDA) and fine mode curvature (FMC) algorithm for retrieving fine mode fraction (FMF) and effective fine mode radius ( $R_{eff,f}$ ), respectively, from *in situ* optical measurements on aerosol particles. Although these algorithms have been applied previously to remote sensing measurements, the work reported here represents the first application to *in situ* optical measurements, allowing an assessment of the accuracy of the retrievals of FMF and  $R_{eff,f}$  through comparisons with other *in situ* measurements that measure FMF and  $R_{eff,f}$  in a more direct manner. The *in situ* techniques for measuring aerosol optical properties include cavity ring-down spectroscopy (extinction coefficient), nephelometry (scattering coefficient) and particle soot absorption photometry (PSAP, absorption coefficient), with measurements made at a variety of wavelengths spanning the visible and near infrared, and for aerosol ensembles using a variety of impactor cut sizes (1  $\mu\text{m}$ , 2.5  $\mu\text{m}$  and 10  $\mu\text{m}$ ). Moreover, fine mode particle size distributions are measured directly using a scanning mobility particle sizer. The reported assessments of FMF and  $R_{eff,f}$  retrieval accuracies are important to those in the remote sensing community and also those seeking to characterise aerosol size distribution properties from *in situ* optical measurements. To this end, the work represents a substantial contribution and is suitable for publication in Atmospheric Chemistry and Physics. I recommend publication after the following comments have been addressed.

We thank the reviewer for their comment on the utility of this work towards the remote sensing community.

### Specific comments

Line 160: It would be good if the authors could be more specific as to how biomass burning confounds the expectation of an anthropogenic-associated fine mode and a coarse mode associated with natural emissions. In particular, the authors reference Hamill *et al.* 2016, but it would be useful for the authors to be more specific about what this study reported that is relevant to the current argument.

We have added the following text to the manuscript to clarify: "*In particular, it can be difficult to distinguish biomass burning particles from particles derived from urban sources, as both primarily fall within the fine mode and are somewhat absorbing.*"

Line 204: Please could the authors explain what is meant by ‘polar angle representation of  $\alpha^f$  vs  $\alpha^c$ . In particular, it would be useful if this representation could be plotted using some of the extinction data later reported for the reader to visualise. Moreover, the van de Hulst parameter and how it is calculated from optical data using the polar plots referred to should be explained more clearly to provide the reader with greater clarity and tools for understanding the results later in the text. In my view, this is one change that would greatly improve understanding readability and understanding, and simply referring the reader to O’Neil et al. 2005 to get all the necessary theoretical details is not helpful. Perhaps, if such a discussion is too long for the main text, a discussion on the polar representation and example plots could be provided in the supplementary information.

We have extensively revised the text near line 204 to attempt to clarify the statement about the polar representation and to provide further details regarding interpretation. We considered adding a figure similar to that shown in O’Neill et al. (2005), shown below. The figure itself is exceptionally complex, and thus we have decided to not include a new figure (either in the main text or supplemental).

The extinction and its first and second derivatives are determined from the fit at a reference wavelength of 500 nm, *a common reference wavelength along with 550 nm in optical studies*. The first derivative (i.e. slope) is denoted  $\alpha$  in analogy to the Ångström exponent, but in this non-linear, second order approach it is a function of wavelength. The second derivative  $\alpha'$  (i.e. spectral curvature) may, in principle, be wavelength dependent over the observed range, but using a second order polynomial fit yields a *constant value*. Values of  $\alpha$  and  $\alpha'$  associated with the fine mode and the coarse mode are indicated using subscript f or c, respectively. In this work, only a second order fit is possible because only three measurements are used to define the wavelength dependence. In the SDA-FMC approach, the observed spectral derivative ( $\alpha$ ) is *used along with the SDA-derived fine mode spectral derivative ( $\alpha_f$ ) to produce the fine mode fraction of extinction (FMF), given as:*

$$FMF = \frac{\alpha - \alpha_c}{\alpha_f + \alpha_c} \quad (1)$$

*Ultimately, the fine mode slope and curvature are both used in the FMC algorithm to determine the fine mode effective radius (discussed in the next section).*

*The algorithm prescribes constant values of the spectral slope and curvature for all coarse mode aerosols ( $\alpha_c$  and  $\alpha'_c$ ) at the reference wavelength of 500 nm. Specifically,  $\alpha_c = -0.15 \pm 0.15$  and  $\alpha'_c = 0.0 \pm 0.15$ , with the uncertainties as per O’Neill et al. (2003). O’Neill et al. (2001) showed that an assumption of an aerosol size distribution with two distinct modes yields a series of three*

*equations that express the relationships between the observed parameters (AOD or extinction coefficient,  $\alpha$ ,  $\alpha'$ ) and their fine and coarse mode analogues. Specifically, the equations can be inverted to yield the fine mode spectral derivative, the fine mode curvature ( $\alpha_f'$ ) and the fine and coarse mode AOD or  $b_{\text{ext}}$  values. It should be noted that the fitting of a 2<sup>nd</sup> order polynomial to input AOD or  $b_{\text{ext}}$  spectra is only an approximation relative to a higher order polynomial. The use of a 2<sup>nd</sup> order polynomial represents a compromise between higher order spectral polynomials being better representations of theoretical Mie spectra and the beneficial damping effects of lower order polynomials in the presence of noisy spectra (O'Neill et al., 2001). The observationally determined total and fine mode spectral derivative and proscribed coarse mode spectral derivative are then used to calculate the fine mode fraction of extinction at the reference wavelength (here 500 nm) using Eqn. 2.*

#### **Estimation of the Fine Mode Effective Radius – the Fine Mode Curvature (FMC) approach**

*Using the SDA-derived, fine mode spectral derivatives ( $\alpha_f'$  and  $\alpha_f$ ), an estimate of the fine mode effective radius is obtained. The basis for this approach is a fundamental parameterization involving the effective van de Hulst phase shift parameter for fine mode aerosols and its representation in  $\alpha_f'$  versus  $\alpha_f$  space. Full details are provided in O'Neill et al. (2005) and O'Neill et al. (2008), and only a summary of the parameterization is provided here. The van de Hulst parameter for the fine mode,  $\rho_{\text{eff},f}$ , is given by:*

$$\rho_{\text{eff},f} = 2 * \frac{2\pi R_{\text{eff},f}}{\lambda} |m - 1| \quad (2)$$

*where  $\lambda$  is the reference wavelength and  $m$  is the complex refractive index at that wavelength (O'Neill et al., 2005). An estimate of this purely optical parameter is based on a 3<sup>rd</sup> order polynomial derived from numerical Mie simulations that relate  $\rho_{\text{eff},f}$  and the polar angle ( $\psi$ ) coordinate of any point in  $\alpha_f'$  vs.  $\alpha_f$  space (O'Neill et al., 2005). The value of  $\psi$  for any given retrieval is simply the arctangent of  $\alpha_f'$  divided by  $\alpha_f$  (minus small prescribed offsets of  $\alpha_{f,0}'$  over  $\alpha_{f,0}$  respectively). Individual simulated contour curves of  $\alpha_f'$  versus  $\alpha_f$  correspond to particle size distributions of differing  $R_{\text{eff},f}$  for constant values of refractive index and were illustrated in Figure 1 of O'Neill et al. (2005). The three different “lines of constant  $\rho_{\text{eff},f}$ ” in that figure correspond to three different values of  $\psi$  (where both  $\rho_{\text{eff},f}$  and  $\psi$  increase in the counterclockwise direction from the horizontal). The  $R_{\text{eff},f}$  values are then computed from the*

retrieved value of  $\rho_{eff,f}$ , by inverting equation (3), if the refractive index of the particles is known. Since the refractive index is generally unknown for the situations we consider here, the information provided by this approach is actually a combination of size and composition. In many cases, an average, constant value for the real portion of the refractive index can be assumed and the imaginary part neglected to provide an estimate of the effective radius; this is, in part, because the imaginary component is typically much smaller than the real component of the refractive index, and thus the  $R_{eff,f}$  value is relatively insensitive to variations in the imaginary component. This treatment is questionable if strong changes in the average composition that lead to changes in  $m$  are suspected. For example if the composition shifted from pure sulfate aerosol ( $m = 1.53 + 0i$ ) to a brown carbon organic ( $m = 1.4 + 0.03i$ ) this would introduce a 33% shift in the derived radius with no change in actual size; the majority of this shift in the derived radius *results* from the change in the real component of the refractive index.

*The FMC method represented by the inversion of equation (3) has been less rigorously validated than the SDA portion and is expected to be more susceptible to problems related to measurement errors and a decreasing sensitivity with decreasing fine mode fraction of extinction. The FMC validation is largely confined to comparisons with the more comprehensive AERONET inversions of Dubovik and King (2000), referred to henceforth as the D&G inversions. These inversions, which require the combination of AOD and sky radiance data, are of a significantly lower frequency than simple AOD measurements. The sky radiance data are collected nominally once per hour while AOD measurements are made once every 3 minutes. Comparisons between the FMC method and the D&G inversions show averaged FMC versus AERONET differences of  $10\% \pm 30\%$  (mean  $\pm$  standard deviation of  $(\rho_{eff,f,FMC} - \rho_{eff,f,D\&K}) / \rho_{eff,f,D\&K}$ ) for large FMF values  $> 0.5$ , at least for the limited data set of O'Neill et al. (2005) and confirmed by more recently unpublished AERONET-wide comparisons between the FMC and D&G methods.*

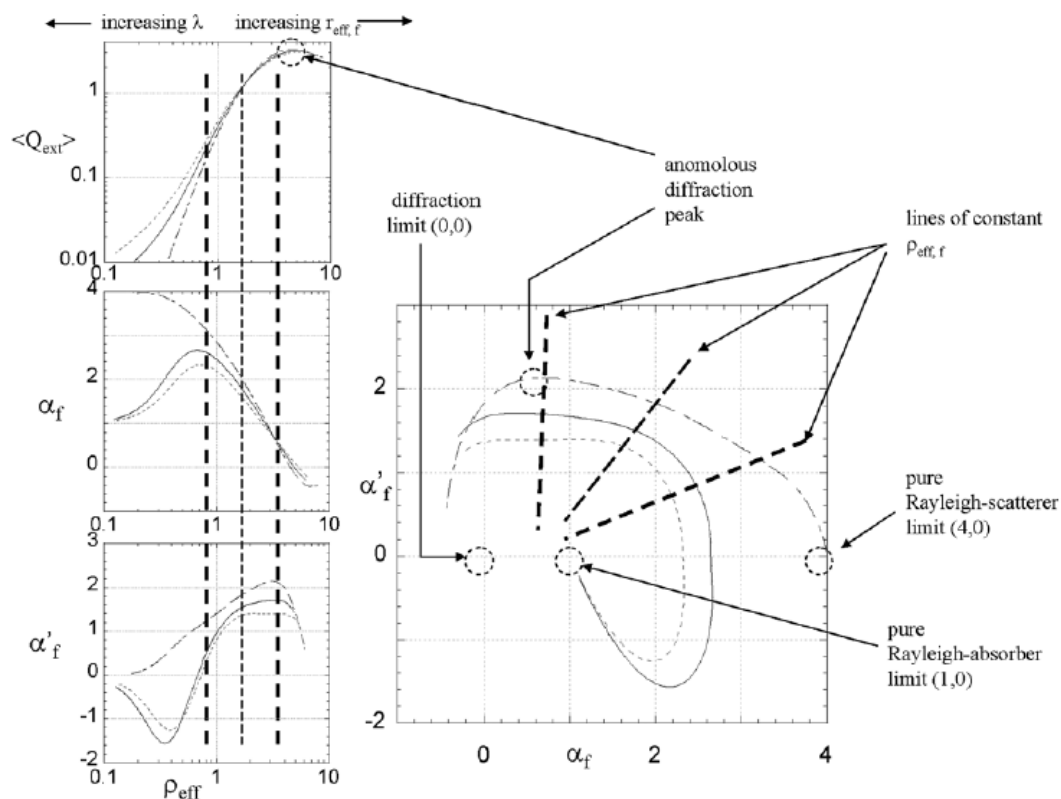


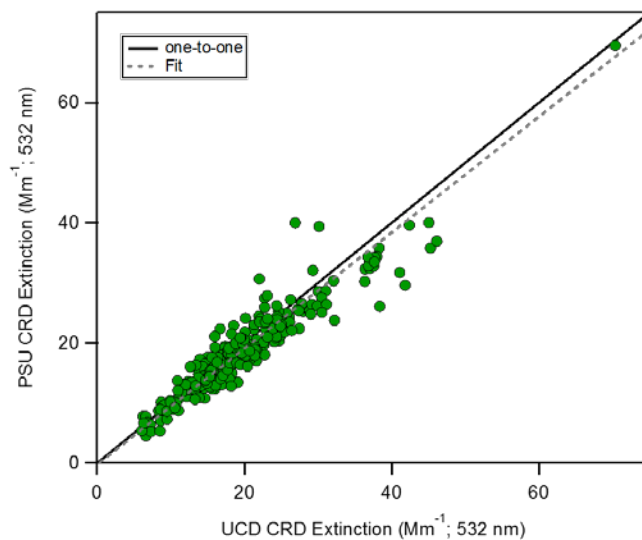
Fig. 1 from O'Neill et al. (2005).

Lines 322 – 326: The best-fit slope is 0.87. I'm surprised that the agreement is not better and be closer to a 1:1 relationship. Is the high noise, associated with the poorer precision in the PSU measurements, responsible for this deviation? Please could the authors describe why the PSU CRDS is less precise and state in clear terms that the data from the PSU instrument is neglected in further analysis here because of this poorer precision. Also, for the aforementioned reasons (poor slope of 0.87 and poor precision in PSU 532-nm CRDS data), I do not agree with the phrase '...the two instruments were measuring the same aerosol with comparable measurement quality...'.

The reviewer raises an important point about comparability between the two instruments. First, we have deleted the phrase mentioned by the reviewer ("...the two instruments..."). Second, more importantly, we note that the original fit was performed using a standard linear regression. However, because there is uncertainty in both the x and y it is more appropriate to use an orthogonal distance regression (ODR) fit. The slope from an ODR fit (performed in Igor Pro using the ODR=2 command) yielded an improved slope of 0.96 and an intercept of  $-0.2 \pm 0.25$ , i.e. indistinguishable from zero. (We note that this revised slope is consistent with that obtained if a ratio is taken between the measurements two instruments, and then a Gaussian curve is fit to a histogram of the ratios. This indicates the appropriateness of the ODR fit.) This slope is within the measurement uncertainty of the two instruments. The figure and discussion in the text have been updated accordingly.

The difference in precision between the instruments most likely results from differences in instrument design, electronics, alignment and mirror quality. While precision is certainly a concern, for our analysis the accuracy, as assessed by the comparability between the UCD and PSU instruments, is more important. Poorer precision in the PSU measurements will translate to lower precision in the derived FMF and fine mode effective radius. However, the overall trends and the average behavior would be unaffected by the poorer precision, so long as the two instruments agree on average (which they do). We have revised the text as follows, and updated Fig. S1.

To obtain three-wavelength bext measurements for use in the SDA-FMC analysis, we combined the measurements from the two CRD instruments (*the 1064 nm measurements from the PSU instrument were used with the 532 nm and 405 nm UCD data after all had been averaged to one-hour*). To assess whether this was a reasonable approach, the 532 nm time series data from the two instruments were overlaid and examined for differences. There is a high degree of temporal correspondence between the measurements from the two instruments, although there was a clear difference in precision, with the UCD CRD having approximately 3 times better precision than the PSU instrument at comparable integration times. This difference in precision results from differences in instrumental design and (likely) mirror quality. A scatterplot (Figure S1) of  $b_{ext,PSU}$  versus  $b_{ext,UCD}$  also showed good correlation, with a best fit line from an orthogonal distance regression fit having a slope = 0.96 and an intercept that was statistically indistinguishable from zero. This is within the uncertainties of the instruments. The good agreement at 532 nm between the PSU and UCD instruments suggests that combining the 1064 nm measurements from PSU with the 405 nm and 532 nm measurements from UCD is reasonable. If the very slight low bias in the 532 nm  $b_{ext}$  from PSU relative to the UCD measurements applies to the 1064 nm measurements then the derived FMF values might be slightly overestimated.



Line 334: What is the basis for an inverse wavelength dependence? A reference showing that inverse wavelength dependence is a reasonable approximation would also be useful here.

We have modified this to say “The absorption coefficients were *interpolated* to the nephelometer wavelengths assuming the inverse wavelength dependence characteristic of uncoated black carbon as appropriate for this region (Cappa et al., 2016).”

Lines 401 – 403: The authors discuss errors in  $R_{eff,f}$  (later in the text) that arise in part from 5% errors in cavity ring-down extinction measurements. However, no consideration is given to the uncertainties that arise in FMF or  $R_{eff,f}$  from errors in the summation (scattering + absorption) data. Given the very large uncertainties and biases that exist in filter-based measurements of absorption, such as from a PSAP, can the authors comment on the corresponding uncertainties in their FMF and  $R_{eff,f}$  retrievals when using the summation method. Have the authors considered the influence of absorption correction schemes for filter-based absorption measurements?

As the reviewer notes, absorption measurements from PSAP instruments can be biased, typically high (Cappa et al., 2008; Lack et al., 2008). The campaign average SSA at 532 nm for T0 was 0.87, as measured by the UCD CRD and photoacoustic instrument (Cappa et al., 2016). This is actually very similar to that obtained from the PSAP + Neph (0.89). The literature cited above suggests biases up to perhaps a factor of two are possible, although based on the conditions during CARES lower values would be expected. Assuming a factor of two positive bias in the PSAP absorption, the extinction would change (decrease) by 5%. However, important to the current study, the potential bias in the PSAP is not thought to be especially wavelength dependent. The method used here relies on spectral curvature and not on the absolute extinction. Thus, if all of the extinction measurements were 5% lower then the curvature would be unaffected. Put another way, if there is a systematic, wavelength-independent bias in the measurements then the impact on the derived FMF and  $R_{eff,f}$  would be small. If the bias were strongly wavelength dependent, then the resulting FMF and  $R_{eff,f}$  would be impacted.

#### **Technical comments:**

Line 19: To reinforce that the ground based measurements are *in situ* opposed to ground based remote sensing, it would be effect to use the phrase ‘Multi-wavelength *in situ*...’ in the opening sentence.

Done

Line 24, ‘*Application to in situ measurements allows for comparison...*’: This is a bit ambiguous. Please can the authors specify what is being applied to the *in situ* measurements (the SDA and FMC algorithms). Also, please specify the quantities being compared when stating ‘...for comparison...’.

Done

Line 78: Brackets are not required. In any case, full stop should be after end bracket rather than before.

Done

Line 79: There is some ambiguity here. Please specify what is meant by 'former' and 'latter'. In part, this ambiguity is magnified by the inclusion of the preceding statement concerning the list of symbols and acronyms.

Done

Line 99: The phrase is brackets is unclear. What does the eta symbol represent? It doesn't appear in the rest of the text. What is 'ibid'? Also, full stop after the end brackets rather than before.

We have removed this parenthetical. (Ibid is used to refer to the previous reference, but we no longer use this in the manuscript.)

Line 99 – 101: This sentence is confusing on first read as it suggests that the fine mode spectral derivatives can be used with equation 1 to calculate  $Reff,f$ . In actual fact, the authors are saying that the spectral derivatives can be used to calculate  $Reff,f$  using a fine mode curvature algorithm, although a strict definition of  $Reff,f$  in terms of the number size distribution is provided by equation 1. Perhaps, a suitable rewording would be 'The fine mode spectral derivatives can then be used to obtain the effective radius for the fine mode through a fine mode curvature algorithm. Alternatively, the fine mode effective radius can be calculated from direct measurements of size distribution (e.g. from scanning mobility particle sizer) using equation 1 (Hansen and Travis (1974)):'.

Thank you for the suggestion. We have adopted the suggested text.

Line 108: There is some ambiguity here. Please specify that it is particle size information from SMPS data that is included in the integration.

Done

Line 114: Please specify that the methods are 'Numerical methods'. Also, please amend text to state that these 'numerical methods' are not *for* remote sensing measurement, rather are *applied* to remote sensing data.

Done

Line 138: For readability, the authors might want to move the sentence on lines 143 – 144 to after line 138 '...complementary *in situ* measurements.' to describe the direct measurements of  $Reff,f$  that the authors perform. Also, mention here that optical measurements of impactor-selected portions of the aerosol ensemble were performed to measure FMF directly.

Done

Lines 141 – 143: Brackets not required.

Done

Line 180 – 183: Could the authors make it clearer that  $\alpha$  is the spectral derivative for the whole aerosol sample, while  $\alpha_f$  is that measured when an impactor is used to remove coarse mode contributions.

This is a slight misunderstanding. Both come from the optical data – the fine version is a result of the SDA part of the procedure. We have clarified this as follows: “In the SDA-FMC approach, the observed spectral derivative ( $\alpha$ ) is combined with the *SDA-derived fine mode spectral derivative ( $\alpha_f$ )* to produce the fine mode fraction of extinction. The fine mode slope and curvature are both used in determining the fine mode effective radius.”

Line 181, ‘...is combined with...’: This is ambiguous. How are  $\alpha$  and  $\alpha_f$  combined? This is unclear to the reader at this early stage in the text. An equation to define FMF in terms of  $\alpha$  and  $\alpha_f$  would be useful here. Indeed, this equation is equation (2) later in the text. Could the authors move equation 2 to this point and define FMF here.

We have moved Eqn. 2 up to this point, and clarified the text (see response above).

Line 189: What is meant by ‘modality’? Please could the authors clarify the text here.

Referring to the two modes. We have modified to “An assumption of an aerosol size distribution with two distinct modes yields...”

Line 189: What ‘measurements’ are the authors referring to? Size distribution measurements, perhaps.

Yes. We have modified the text to make this clearer.

Line 190: Could the authors give these three equations? What are the dependent variables?

We have expanded the discussion slightly here, as discussed above in relation to understanding the curvature.

Line 188 – 191: This whole sentence is vague, difficult to read and needs clarifying. What is meant by ‘approximation level relative to a theoretical Mie representation’ and ‘limited to second order’?

We have clarified this as: “*Specifically, the equations can be inverted to yield the fine mode spectral derivative, the fine mode curvature ( $\alpha_f$ ) and the fine and coarse mode AOD or bext values. It should be noted that the fitting of a 2nd order polynomial to input AOD or bext spectra is only an approximation relative to a higher order polynomial. The use of a 2nd order polynomial represents a compromise between higher order spectral polynomials being better representations of theoretical Mie spectra and the*”

*beneficial damping effects of lower order polynomials in the presence of noisy spectra (O'Neill et al., 2001)."*

Line 193: Is the set of three equations referred to here the same as the 'three succinct equations' referred to on line 190? If so, please clarify in the text.

Please see response to previous comment.

Line 196: Please specify reference wavelength. I believe this is 500 nm, but please specify to remove any doubt.

done

Line 209: What is 'ibid'?

We have removed all references to *ibid*.

Line 210: There is ambiguity here. What is meant by 'this' in 'estimate of this purely optical parameter...'. Presumably, 'this' is referring to the van de Hulst parameter, but the authors should be more specific here to remove doubt.

This has been clarified.

Lines 225 – 226: Ambiguity; it is not clear what is meant by 'polar-coordinate system relationship'. Moreover, the phrase 'near monotonic fit' is also ambiguous; a near monotonic fit of what function?

We have extensively revised the text near line 204 to attempt to clarify the statement about the polar representation and to provide further details regarding interpretation. We provide above the detailed changes to this section.

Line 228: Brackets around reference not needed.

We have reworded and removed the brackets.

Line 230: Ambiguity; please specify what is being compared in 'The comparisons...'.

We have reworded to clarify. The modified text reads:

*The sky radiance data are collected nominally once per hour while AOD measurements are made once every 3 minutes. Comparisons between the FMC method and the D&G inversions show averaged FMC versus AERONET differences of  $10\% \pm 30\%$  (mean  $\pm$  standard deviation of  $(\rho_{\text{eff},f,\text{FMC}} - \rho_{\text{eff},f,\text{D\&K}}) / \rho_{\text{eff},f,\text{D\&K}}$ ) for large FMF values  $> 0.5$ , at least for the limited data set of O'Neill et al. (2005) and confirmed by more recently unpublished AERONET-wide comparisons between the FMC and D&G methods.*

Line 246: What is meant by 'expensive'? Computationally expensive, or expensive in monetary terms?

The latter. As we are discussing physical equipment at this point, we believe the use is sufficiently clear.

Line 296: Remove brackets around reference.

Done.

Line 340: Lower case 'N' in nephelometer.

Done

Line 425: Do the authors mean extinction, instead of scattering? For the cases of aerosols sampled here, it probably does not matter. But, with the authors preferring *extinction* throughout the manuscript, it would be good to be consistent.

We have modified this to read: "Nonetheless, since the major sources of fine and coarse mode particles are likely to be reasonably distinct in many environments, the FMFext,CRD can provide a characterization of the variability in the contributions of such sources to the total *extinction* and, in environments where the extinction is dominated by scattering (i.e. when the SSA is large), to the total scattering as well."

Line 538: Full stop (period) required after 'fine mode distribution'.

Done

## Reviewer #1

### General comments

The manuscript presented by Atkinson et al. describes the retrieval of particle size related information from multi-wavelength aerosol extinction, scattering and absorption field measurements using spectral deconvolution method that is typically used in remote sensing applications. The authors aim to compare the retrieved values with values that are calculated directly from size distribution measurements in order to validate the retrieval approach and to discuss its limitations. This work contains substantial contribution to further verification of remote sensing measurements using in-situ instruments. I recommend publication after the following comments have been addressed. Most importantly, as the main goal of this work is to evaluate the spectral deconvolution algorithm by comparison to size distribution measurements an additional effort should be made by the authors to describe and present the error propagation or uncertainty calculation inherent to each calculation from the uncertainties in each measured parameter.

We thank the reviewer for the comment about error propagation and uncertainty. We have worked to clarify and add to this aspect of our work.

### Specific and technical comments

1) Line 232: "...averaged AERONET-SDA differences of 10% +/- 30% for large FMF values > 0.5". It is not clear if the authors mean a difference of -20% to +40% or from 0% to +40%?

This has been clarified as:

"Comparisons between the FMC method and the D&K [Dubovik and King] inversions show averaged FMC versus AERONET differences of  $10\% \pm 30\%$  (mean  $\pm$  standard deviation of  $(\rho_{\text{eff},f,\text{FMC}} - \rho_{\text{eff},f,\text{D\&K}}) / \rho_{\text{eff},f,\text{D\&K}}$ ) for large FMF values > 0.5, at least for the limited data set of O'Neill et al. (2005) and confirmed by more recently unpublished AERONET-wide comparisons between the FMC and D&K methods."

2) Line 254: since measurement of aerosols light extinction are by definition only apply to the forward direction it is unclear what the authors mean by truncation errors in CRD?

We have modified this to:

"Cavity ring-down measurements *directly quantify total extinction within the cavity, which is contributed from both gases and particles (Smith and Atkinson, 2001; Brown, 2003). To determine extinction by aerosols only, the entering air stream is periodically directed through a filter such that a gas-only reference is determined. Extinction by aerosol particles is determined relative to this gas zero. The aerosol*

*extinction is further corrected to account for the practical aspect that the complete mirror-to-mirror distance of the optical cavity is typically not filled with aerosols (to keep the mirrors clean) (Langridge et al., 2011)."*

3) Line 313: data in table 1 regarding the PSU-CRD does not correspond to the text.

We have clarified the capabilities of the PSU-CRD so that the text and table are consistent. The table now indicates that the PSU-CRD measures also at 532 nm. However, it should be noted that for our analysis for the T0 site, the 532 nm data from the UCD CRD-PAS instrument was used, not the PSU-CRD 532 nm data.

4) Line 323: a slope of 0.87 in the correlation between two CRD instruments at the same wavelength is significant. What is the uncertainty on this value? How was this 13% error mitigated in the data analysis? Was any correction applied? And how sure are the authors that the same "error" would apply to the 1064nm or the 405 nm CRD's? The authors are sure that with this 13% difference between the instruments "the two instruments were measuring the same aerosol with comparable measurement quality". I do not agree with this statement.

A similar concern was raised by the previous reviewer. We repeat our response here, and note that we have removed the statement about "measurement quality." Regarding the comparability between 532 nm and 1064 nm, the measurements were made for particles sampled through the same inlet, and thus we expect any differences observed for one channel of this instrument to be similar for the others, given that the main reason for differences between the UCD and PSU CRD instruments is particle losses.

From above: The reviewer raises an important point about comparability between the two instruments. First, we have deleted the phrase mentioned by the reviewer ("...the two instruments..."). Second, more importantly, we note that the original fit was performed using a standard linear regression. However, because there is uncertainty in both the x and y it is more appropriate to use an orthogonal distance regression (ODR) fit. The slope from an ODR fit (performed in Igor Pro using the ODR=2 command) yielded an improved slope of 0.96 and an intercept of  $-0.2 \pm 0.25$ , i.e. indistinguishable from zero. (We note that this revised slope is consistent with that obtained if a ratio is taken between the measurements two instruments, and then a Gaussian curve is fit to a histogram of the ratios. This indicates the appropriateness of the ODR fit.) This slope is within the measurement uncertainty of the two instruments. The figure and discussion in the text have been updated accordingly.

5) Line 343-350: SMPS scans typically take several minutes. A car passing by or a wind gust will cause significant changes to the aerosols population in time scales of seconds. This can be verified by looking at total aerosols concentration data taken with a CPC with a 1 sec resolution. To overcome mid-scan dramatic changes some dead volume is typically applied to allow for mixing of the aerosols and to smooth rapid changes. What measures were taken to insure that each individual SMPS scan is not interrupted by such events?

First, there is a substantial amount of volume in the sampling masts and the internal plumbing in the trailers, which helps to smooth out fast fluctuations. In looking at the e.g. CPC data (or the extinction observations at their native time resolution of 2 seconds) we find that there are very few periods where plumes, such as that from a car, were sampled. Thus, when the SMPS observations are averaged over an hour, as we have done here, issues related to a single scan will average out. Certainly if we were using each individual SMPS scan, rather than an hour average, plumes would be a larger concern. Further, we note that in Atkinson et al. (2015) we explicitly compared the absolute extinction measurements from to the extinction calculated from the size distribution measurements. Overall, strong linear correlations were observed for the dry extinction with little evidence of outliers that might have resulted from SMPS issues.

6) All figures should have some indication of the uncertainty of the presented values in order for the reader to appreciate the variation in the data within/between data series and temporal variation such as the diurnal cycle.

We have updated the figures to have indications of uncertainty. Further discussion about uncertainties is provided in response to Reviewer #3.

7) Lines 398-399: the authors claim that the difference between FMFCRD and FMFsum is due to significant contribution by large particle. Wouldn't it be possible to find some support for this claim in the SMPS data?

The SMPS measurements only go up to ~ 800 nm, limiting the ability of the SMPS to provide information on large-particle contributions. However, we note that Kassianov et al. (2012) and Cappa et al. (2016) both discuss at length the large contribution from coarse mode particles to the extinction during CARES. Thus there is very good reason to think that large particles contribute to the difference.

8) Lines 419-423: I am afraid I don't understand how the differences between the two sites (and not the difference between CRD and SUM in site T0) "highlights the fact that there is not a precise definition of "fine" and "coarse" in terms of a specific size cut in the optical method." Additionally it is not clear what do the authors mean by the shape of the size distribution. Is it the width and/or amplitude ?

What we mean is that when a property such as "fine mode fraction" is retrieved from remote sensing measurements in different locations or even at different times, the meaning of "fine mode" may change somewhat. The characteristic particle size that distinguishes between those in the "fine" and those in the "coarse" mode is not a constant and will vary based on the particular mix of sources and the nature (e.g. shape, number of actual modes) of the overall size distribution. Also, by "shape" we mean width, position and number of actual modes. We have worked to clarify the discussion as follows:

*"However, the results demonstrate that the optical method does not allow for a precise definition of "fine" and "coarse" in terms of a specific, effective size cut that*

*distinguishes between the two regimes. While the SMF has an explicitly defined size cut (PM1), the effective size cut for the FMF can vary. The effective size cut is dependent on the shapes (i.e. widths, positions and number of actual modes) of the size distributions in the “fine” and “coarse” size regimes and the extent of overlap between them, which is dependent on the size range of particles sampled (e.g. PM2.5 versus PM10). For remote sensing measurements, the particular size that distinguishes between the fine and coarse mode therefore likely varies between locations and seasons.”*

9) In figure 4 errors are needed to establish if the temporal variability is real or within uncertainty. This is important for conclusions presented in lines 461-463 and 477-478.

We have added error bands to Fig. 4. The uncertainties were determined using a Monte Carlo-type approach in which each input to the calculations was varied randomly and independently about its mean, and with a weighting determined from the uncertainty in the input variable.

10) Figure 5: why is the discrepancy mostly clear in the first half of the day then the second half of the day in site T0?

This likely reflects a shift in the effective size cut associated with the FMF. Below we show the diurnal profile of the surface-area weighted size distribution. There is clearly a notable mode right around 1 micron in the early morning/late night periods. When this contributes substantially, the optically-derived  $Reff,f$  is impacted (and shifted towards larger values) while the size-distribution derived  $Reff,f$  is affected to a lesser extent. At T1 this larger mode is much less evident and thus contributes less to the optically-derived  $Reff,f$ . Overall, the difference has to do with the extent to which the “coarse” mode penetrates into the “fine” mode. We have added the figure below to the supplemental material. For these distributions, we have combined the SMPS data with the APS data. Because of limited data available for the APS at the T0 site (due to an instrument malfunction) the size distributions are for only a subset of the total period examined in this manuscript (6/16-6/22). We have added discussion to the main text, where we already had included discussion related to the nucleation mode that is observed during the daytime and that also influences the diurnal behavior.

*“In addition, for T0 there is a notable mode in the surface-area weighted distribution at ~1 micron that is most evident in the early morning (Figure S3). This mode has little influence on the  $Reff,f$  values determined from the size distributions, but contributes to the higher optically determined  $Reff,f$  values in the early morning for T0. This mode is much less prevalent at the T1 site, and thus there is better correspondence between the size-distribution and optical methods.”*

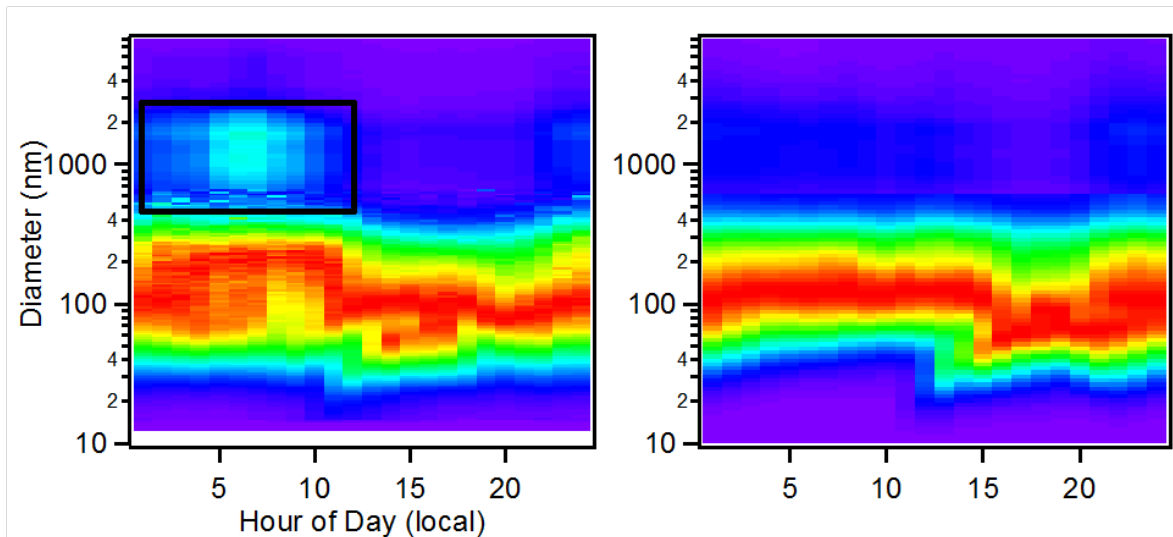


**Figure S3.** Observed diurnal variation for (left) the T0 site and (right) the T1 site for the surface-area weighted size distribution. Distributions have been normalized to the maximum surface area concentration for each hour of the day. The black box shown for T0 highlights the presence of a mode near 1 micron.

## Reviewer #3

This manuscript describes a spectral deconvolution and fine mode curvature method that can retrieve particle size and determine relative contribution of the fine mode particles to the total particle extinction from Multi wavelength aerosol extinction, absorption and scattering measurements. Typically this method is used in remote sensing applications but authors extended the application of this method to in-situ measurements to retrieve particle size. The authors used extinction data from cavity ring down measurements, scattering data from nephelometer and absorption data from particle soot absorption photometer measurements. Overall, the manuscript is clearly written, some suggested clarifications are listed below. I understand this is more of a technique based manuscript but little bit more discussion about the science would be useful. I recommend this paper for publication. However, prior to acceptance, the authors should address the following questions/ suggestions and modify the manuscript accordingly.

My main concern here is about the error analysis in the retrieved size and contribution of the fine mode particles to the total particle extinction. What are the errors on the estimates? A range of relative uncertainties are stated towards the end of the manuscript but it is not clear to me if the authors consider propagation of errors from the measurements.

We thank the reviewer for pushing us to consider our uncertainties to a greater extent. In response, we have added the following text as a new section and updated the figures.

*The uncertainty in the SMF has been estimated from standard error propagation of the uncertainties in the  $PM_{1}$  and  $PM_{10}$  extinction measurements. The assumed uncertainties in  $b_{ext,PM1}$  and  $b_{ext,PM10}$  are  $\pm 1 Mm^{-1}$ . This uncertainty estimate accounts only for random errors, not systematic errors.*

*Uncertainties in the FMF have been estimated based on the uncertainties in the inputs to the SDA-FMC procedure, namely the  $b_{ext}$  values. The assumed uncertainties in the input  $b_{ext}$  were instrument specific:  $<1 Mm^{-1}$  for the UCD CRD,  $1 Mm^{-1}$  for the nephelometer plus PSAP and PSU CRD at T0, and  $3 Mm^{-1}$  for the PSU CRD at T1. The input uncertainties are propagated through the various mathematical relationships using standard methods. The FMF error estimate includes some of the factors that contribute systematic uncertainty in the method. As noted in the Theoretical Approach section, FMF values from the SDA-FMC procedure have been shown to agree well with those determined from the more comprehensive inversion method of Dubovik and King (2000).*

*Uncertainties in the derived  $R_{eff,f}$  are also estimated from the uncertainties in the input values. The size-distribution derived  $R_{eff,f}$  values depend on the SMPS measurements. The SMPS instruments were calibrated (using 200 nm polystyrene latex spheres) prior to the campaign and*

*a drier was used to keep the aerosol RH < 30% throughout the entire campaign. Periodic checks throughout the campaign indicate consistent sizing performance to within 5%. The size distribution data used here were corrected for DMA transfer function, the bipolar charge distribution, the CPC efficiency and internal diffusion losses. Under these conditions the estimated uncertainties for  $D_p$  are around 10% for the size range between 20 and 200 nm (Wiedensohler et al., 2012). Although larger uncertainties could exist for smaller and larger particle sizes, the derived  $R_{eff,f}$  values fell primarily in this range. The estimated SMPS uncertainty (Wiedensohler et al., 2012) was estimated based on intercomparisons between different SMPS instruments and thus probably represents both determinate and indeterminate errors. The relative uncertainty in the  $R_{eff,f}$  from the size distribution measurement is thus estimated to be 10%. This estimate mainly reflects uncertainties in the absolute size, since there is expected to be significant cancellation in the errors produced by the particle counter (the same data are used in the numerator and denominator of Eq. 1).*

*Estimating the uncertainty in the  $R_{eff,f}$  from the SDA-FMC is more challenging because the uncertainties cannot be simply propagated through the equations. Therefore, an approach was taken wherein a large number of  $R_{eff,f}$  values were calculated from input  $b_{ext}$  that were independently, randomly varied within one standard deviation of the measured value, assuming a normal distribution of errors. Potential uncertainty or variability in the real refractive index was accounted for based on the compositional variation (Atkinson et al., 2015) and assuming volume mixing applies. The standard deviation (1s) was 0.015. This is likely a lower estimate of the uncertainty in the RI, as it does not account for absolute uncertainty in the estimate. The standard deviation of the derived  $R_{eff,f}$  is taken as the uncertainty. This Monte Carlo-style approach does not incorporate systematic error sources. The relative uncertainty in the derived  $R_{eff,f}$  is found to range from a few percent up to 40%, depending on the particular instrument suite considered and measurement period. In general, the uncertainties were larger for the PSAP and nephelometer, presumably because the wavelengths used are more closely spaced.*

In the abstract the authors should briefly mention the major limitations of the technique instead of just stating “..some limitations are also identified”. Some of the limitations are mentioned in the text at different places but I suggest providing a list of all the limitations in details at the end so that it would be easier for readers to follow.

We have updated the abstract as follows:

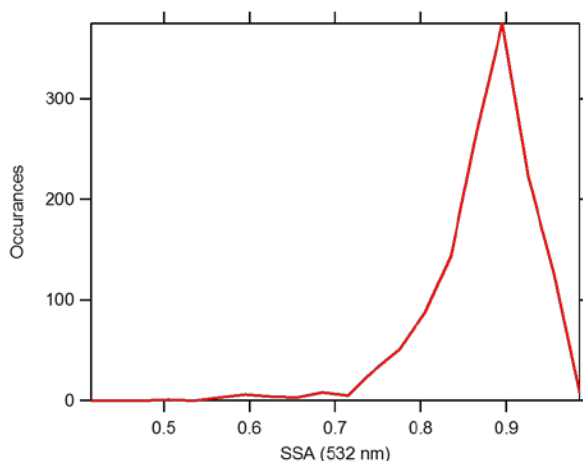
*“Overall, the retrieved fine mode fraction and effective radius compare well with other in situ measurements, including size distribution measurements and scattering and absorption measurements made separately for PM1 and PM10, although there were some periods during which the different methods yielded different results. One key reason identified as contributing to differences between methods is the imprecise definition of “fine” and “coarse” mode from the optical methods, relative to instruments that use a physically defined cut-point.”*

Line 177: please provide detail about the polynomial fit that yields a wavelength invariant version.

We have made substantial revisions to this section, as documented in our response to Reviewer #2 above.

Line 220: I think authors should expand the discussion regarding the uncertainty in refractive index. How the estimated size will affect if some of the plumes contain more absorbing particles such as soot? Authors used an average value of real part from previous study. Here authors can propagate the error.

We are using 1h averages, so very short plumes with highly absorbing material will have little influence on the results. If we look at a histogram of SSA values (see below), we see that there is a reasonably narrow distribution with the vast majority of points between 0.8 and 0.95. Using Mie theory as a guide, we find that the imaginary part of the refractive index need only vary from  $\sim 0.004$  to  $0.02$  to produce SSA values in this range. Such variations have a very small impact on the extinction wavelength dependence; it is much more dependent on the real component. That the results are more sensitive to variations in the real part was stated in the manuscript previously: “For example if the composition shifted from pure sulfate aerosol ( $m = 1.53 + 0i$ ) to a brown carbon organic ( $m = 1.4 + 0.03i$ ) this would introduce a 33% shift in the derived radius with no change in actual size; the majority of this shift in the derived radius results from the change in the real component of the refractive index.”



Line 249: Authors mention here about the truncation angel error but it is not clear to me if they incorporated the corrections to the nephelometer data.

We now state: “The scattering coefficients were corrected for truncation error (Anderson and Ogren, 1998) and the absorption coefficients for filter effects (Ogren, 2010).”

Line 253: This part somehow misleading to me “Cavity ring down measurements do not (in principle) need to be calibrated”

We have modified this to: “Cavity ring-down measurements *directly quantify total extinction within the cavity, which is contributed from both gases and particles (Smith and Atkinson, 2001; Brown, 2003). To determine extinction by aerosols only, the entering air stream is periodically directed through a filter such that a gas-only reference is determined. Extinction by aerosol particles is determined relative to this gas zero. The aerosol extinction is further corrected to account for the practical aspect that the complete mirror-to-mirror distance of the optical cavity is typically not filled with aerosols (to keep the mirrors clean) (Langridge et al., 2011).*”

Line 254: “have very small truncation errors”- please provide a number here.

This has been revised. See response to previous query.

Line 310: Authors mentioned about low relative humidity during measurements used here. Was it low also at T1 site? Scattering measurements can be substantially impacted at high RH.

Yes, the RH was low at both sites throughout the campaign, as shown in Zaveri et al. (2012). Something to this effect was mentioned on Line 359: “As with the T0 PSU instrument, the total aerosol system attempts to measure particle extinction at nearly ambient conditions, resulting in low RH (25 – 40 %) throughout most of the campaign, as measured by an integrated RH/T sensor (Vaisala HMP70).”

Line 333: “The absorption coefficients were adjusted to the nephelometer wavelengths using an inverse wavelength dependence”- please elaborate.

We have clarified that the absorption coefficients were interpolated, rather than adjusted.

Error bars should be provided in all the figs.

We have updated the figures to include uncertainty estimates.

Line 409: “are very similar in absolute magnitude”-please provide the numbers

Values are now provided in Table 2.

Fig.3- FMF-CRD shows higher fine mode fraction during 06/19 to 06/20. Is it because of the no size cut for the CRD measurements?

During this period the absolute extinction was particularly low, making it challenging to assess. The reviewer’s suggestion is certainly possible. However, we note that with the uncertainties added to the figure it is now apparent that the measurements are the same within the estimated uncertainties.

Please consider to change the scale of the y-axis in Fig. 4. Shorter range would help to visualize the variations.

While we understand the reviewer's suggestion to change the range, we have chosen to maintain the y-axis scales they were, namely varying over the same range for both panels. We have done this to facilitate comparison between the sites.

Fig. 5. Once authors do the error propagation, error bars should be included in the figure.

Error bands have been added (see below).

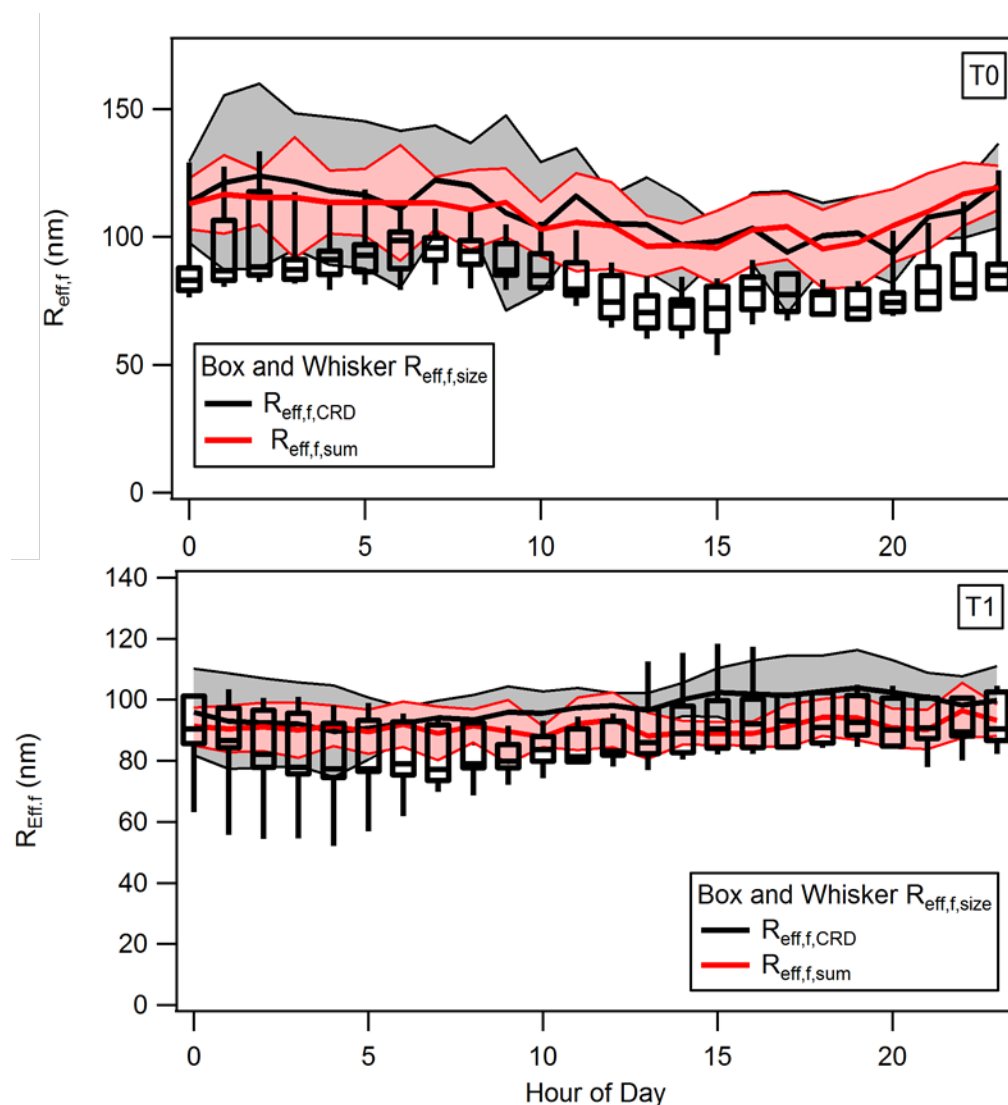


**Figure 5** – The diurnal dependence of  $R_{\text{eff},f}$  for the period shown in Fig. 4 for the (top) T0 and (bottom) T1 sites. The box and whisker plot (bottom and top of box are 5% and 95% of data range, bar is mean, and whiskers extend to full range) shows the results from the direct size distribution measurement ( $R_{\text{eff},f,\text{size}}$ ). The thick lines show the mean diurnal dependence of the optically derived  $R_{\text{eff},f}$ , using the CRD (black) and nephelometer + PSAP (red) measurements. The

light colored bands show the  $\pm 1\sigma$  standard deviation based on the measurement variability over the averaging period.

Is it 1-hr average for the retrieved radius? What would be the minimum integration time for the optically derived radius to achieve a reasonable estimate? In other words, if there is a spike in the data for shorter time, can it be captured?

Yes, it is possible to retrieve estimates of the  $\text{Reff},f$  at higher time resolution and capture spikes. The results at one hour averaging were selected after verifying that the results were not qualitatively different from those with shorter time-scales. We have chosen to focus on the longer term averages, given that remote sensing observations are often used to develop longer-term climatologies for regions and occur in remote regions where short-term spikes are less common. However, in principle shorter time scales can be accessed.

## References

- Anderson, T. L., and Ogren, J. A.: Determining Aerosol Radiative Properties Using the TSI 3563 Integrating Nephelometer, *Aerosol Science and Technology*, 29, 57-69, 10.1080/02786829808965551, 1998.
- Atkinson, D. B., Radney, J. G., Lum, J., Kolesar, K. R., Cziczo, D. J., Pekour, M. S., Zhang, Q., Setyan, A., Zelenyuk, A., and Cappa, C. D.: Aerosol optical hygroscopicity measurements during the 2010 CARES campaign, *Atmos Chem Phys*, 15, 4045-4061, 10.5194/acp-15-4045-2015, 2015.
- Cappa, C. D., Lack, D. A., Burkholder, J. B., and Ravishankara, A. R.: Bias in filter-based aerosol light absorption measurements due to organic aerosol loading: Evidence from laboratory measurements, *Aerosol Sci. Technol.*, 42, 1022-1032, Doi 10.1080/02786820802389285, 2008.
- Cappa, C. D., Kolesar, K. R., Zhang, X. L., Atkinson, D. B., Pekour, M. S., Zaveri, R. A., Zelenyuk, A., and Zhang, Q.: Understanding the optical properties of ambient sub- and supermicron particulate matter: results from the CARES 2010 field study in northern California, *Atmos Chem Phys*, 16, 6511-6535, 10.5194/acp-16-6511-2016, 2016.
- Dubovik, O., and King, M. D.: A flexible inversion algorithm for retrieval of aerosol optical properties from Sun and sky radiance measurements, *J Geophys Res-Atmos*, 105, 20673-20696, 10.1029/2000jd900282, 2000.
- Kassianov, E., Pekour, M., and Barnard, J.: Aerosols in central California: Unexpectedly large contribution of coarse mode to aerosol radiative forcing, *Geophys Res Lett*, 39, L20806, 10.1029/2012GL053469, 2012.
- Lack, D. A., Cappa, C. D., Covert, D. S., Baynard, T., Massoli, P., Sierau, B., Bates, T. S., Quinn, P. K., Lovejoy, E. R., and Ravishankara, A. R.: Bias in filter-based aerosol light absorption measurements due to organic aerosol loading: Evidence from ambient measurements, *Aerosol Sci. Technol.*, 42, 1033-1041, Doi 10.1080/02786820802389277, 2008.
- O'Neill, N. T., Eck, T. F., Holben, B. N., Smirnov, A., Dubovik, O., and Royer, A.: Bimodal size distribution influences on the variation of Angstrom derivatives in spectral and optical depth space, *J Geophys Res-Atmos*, 106, 9787-9806, 10.1029/2000jd900245, 2001.
- O'Neill, N. T., Eck, T. F., Smirnov, A., Holben, B. N., and Thulasiraman, S.: Spectral discrimination of coarse and fine mode optical depth, *J Geophys Res-Atmos*, 108, 4559, 10.1029/2002jd002975, 2003.

O'Neill, N. T., Thulasiraman, S., Eck, T. F., and Reid, J. S.: Robust optical features of fine mode size distributions: Application to the Quebec smoke event of 2002, *J Geophys Res-Atmos*, 110, D11207, 10.1029/2004jd005157, 2005.

O'Neill, N. T., Thulasiraman, S., Eck, T. F., and Reid, J. S.: Correction to the effective radius expression in O'Neill et al. (2005), *J Geophys Res-Atmos*, 113, D24203, 10.1029/2008JD011334, 2008.

Ogren, J. A.: Comment on "Calibration and Intercomparison of Filter-Based Measurements of Visible Light Absorption by Aerosols", *Aerosol Science and Technology*, 44, 589-591, 10.1080/02786826.2010.482111, 2010.

Wiedensohler, A., Birmili, W., Nowak, A., Sonntag, A., Weinhold, K., Merkel, M., Wehner, B., Tuch, T., Pfeifer, S., Fiebig, M., Fjåraa, A. M., Asmi, E., Sellegri, K., Depuy, R., Venzac, H., Villani, P., Laj, P., Aalto, P., Ogren, J. A., Swietlicki, E., Williams, P., Roldin, P., Quincey, P., Hüglin, C., Fierz-Schmidhauser, R., Gysel, M., Weingartner, E., Riccobono, F., Santos, S., Grüning, C., Faloon, K., Beddows, D., Harrison, R., Monahan, C., Jennings, S. G., O'Dowd, C. D., Marinoni, A., Horn, H. G., Keck, L., Jiang, J., Scheckman, J., McMurry, P. H., Deng, Z., Zhao, C. S., Moerman, M., Henzing, B., de Leeuw, G., Löschau, G., and Bastian, S.: Mobility particle size spectrometers: harmonization of technical standards and data structure to facilitate high quality long-term observations of atmospheric particle number size distributions, *Atmos. Meas. Tech.*, 5, 657-685, 10.5194/amt-5-657-2012, 2012.

Zaveri, R. A., Shaw, W. J., Cziczo, D. J., Schmid, B., Ferrare, R. A., Alexander, M. L., Alexandrov, M., Alvarez, R. J., Arnott, W. P., Atkinson, D. B., Baidar, S., Banta, R. M., Barnard, J. C., Beranek, J., Berg, L. K., Brechtel, F., Brewer, W. A., Cahill, J. F., Cairns, B., Cappa, C. D., Chand, D., China, S., Comstock, J. M., Dubey, M. K., Easter, R. C., Erickson, M. H., Fast, J. D., Floerchinger, C., Flowers, B. A., Fortner, E., Gaffney, J. S., Gilles, M. K., Gorkowski, K., Gustafson, W. I., Gyawali, M., Hair, J., Hardesty, R. M., Harworth, J. W., Herndon, S., Hiranuma, N., Hostetler, C., Hubbe, J. M., Jayne, J. T., Jeong, H., Jobson, B. T., Kassianov, E. I., Kleinman, L. I., Kluzek, C., Knighton, B., Kolesar, K. R., Kuang, C., Kubatova, A., Langford, A. O., Laskin, A., Laulainen, N., Marchbanks, R. D., Mazzoleni, C., Mei, F., Moffet, R. C., Nelson, D., Obland, M. D., Oetjen, H., Onasch, T. B., Ortega, I., Ottaviani, M., Pekour, M., Prather, K. A., Radney, J. G., Rogers, R. R., Sandberg, S. P., Sedlacek, A., Senff, C. J., Senum, G., Setyan, A., Shilling, J. E., Shrivastava, M., Song, C., Springston, S. R., Subramanian, R., Suski, K., Tomlinson, J., Volkamer, R., Wallace, H. W., Wang, J., Weickmann, A. M., Worsnop, D. R., Yu, X. Y., Zelenyuk, A., and Zhang, Q.: Overview of the 2010 Carbonaceous Aerosols and Radiative Effects Study (CARES), *Atmos Chem Phys*, 12, 7647-7687, 10.5194/acp-12-7647-2012, 2012.

## 1 Using Spectral Methods to Obtain Particle Size Information from Optical Data: 2 Applications to Measurements from CARES 2010

Style Definition: Heading 2: Font: Bold

3 Dean B. Atkinson<sup>1</sup>, Mikhail Pekour<sup>2</sup>, Duli Chand<sup>2</sup>, James G. Radney<sup>1,\*\*\*</sup>, Katheryn R. Kolesar<sup>5,\*</sup>, Qi Zhang<sup>3</sup>,  
4 Ari Setyan<sup>3,\*\*</sup>, Norman T. O'Neill<sup>4</sup>, Christopher D. Cappa<sup>5</sup>

5 [1] [Department of Chemistry, Portland State University, Portland, OR, USA, 97207]

6 [2] [Pacific Northwest National Laboratory, Richland, WA, USA, 99352]

7 [3] [Department of Environmental Toxicology, University of California, Davis, CA, USA, 95616]

8 [4] [Centre d'Applications et de Recherches en Télédétection, Université de Sherbrooke, Sherbrooke,  
9 Canada]

10 [5] [Department of Civil and Environmental Engineering, University of California, Davis, CA, USA, 95616]

11 \* Now at: Air Sciences, Inc., Portland, OR, 97214, USA

12 \*\* Now at: Empa, Swiss Federal Laboratories for Materials Science and Technology, 8600 Dübendorf,  
13 Switzerland

14 \*\*\* Now at: Material Measurement Laboratory, National Institute of Standards and Technology,  
15 Gaithersburg, Maryland, 20899, USA

16 Correspondence to: D. B. Atkinson (atkinsond@pdx.edu)

17

### 18 Abstract

Formatted: Heading 1

19 Multi-wavelength *in situ* aerosol extinction, absorption and scattering measurements made at two  
20 ground sites during the 2010 Carbonaceous Aerosols and Radiative Effects Study (CARES) are analyzed  
21 using a spectral deconvolution method that allows extraction of particle size-related information,  
22 including the fraction of extinction produced by the fine mode particles and the effective radius of the  
23 fine mode. The spectral deconvolution method is typically applied to analysis of remote sensing

24 measurements. Here, its application to *in situ* measurements allows for comparison with more direct

Deleted: Application

25 measurement methods and validation of the retrieval approach. Overall, the retrieved fine mode

Deleted: Here

26 fraction and effective radius compare well with other *in situ* measurements, including size distribution

Deleted: generally

27 measurements and scattering and absorption measurements made separately for PM<sub>1</sub> and PM<sub>10</sub>,

28 although there were some periods during which the different methods yielded different results. One key

Deleted: but some limitations are also identified.

29 contributor to differences between the results obtained is the alternative, spectrally based definition of

30 "fine" and "coarse" mode from the optical methods, relative to instruments that use a physically

31 defined cut-point. These results indicate that for campaigns where size, composition, and multi-

32 wavelength optical property measurements are made, comparison of the results can result in closure or

33 can identify unusual circumstances. The comparison here also demonstrates that *in situ* multi-

38 wavelength optical property measurements can be used to determine information about particle size  
39 distributions in situations where direct size distribution measurements are not available.

40

41 **Introduction**

42 Aerosols remain a substantial source of uncertainty in climate models, despite considerable progress in  
43 scientific understanding of their chemical, physical and optical properties in the last few decades (IPCC,  
44 2013). As greater understanding has developed in each of these areas, new complexity is also uncovered  
45 and the interconnectedness of the various properties becomes even more evident. Light scattering by  
46 atmospheric particles has a net cooling effect on climate that is one major offset to greenhouse gas  
47 induced climate warming (Charlson et al., 2005; Bond et al., 2011). The efficiency with which the  
48 atmospheric aerosol interacts with electromagnetic radiation (e.g. sunlight) is dependent upon the size,  
49 composition, shape and morphology of the particles. These properties are not static in time, instead  
50 evolving as particles are transported through the atmosphere as a result of chemical processing,  
51 scavenging and changes in the environmental conditions (e.g. relative humidity and temperature)  
52 (Doran et al., 2007; George and Abbatt, 2010; Lack and Cappa, 2010).

53 Characterization of the spatial distribution of aerosol particle concentrations and properties is important  
54 to assessing their impact on the atmospheric radiation budget through direct aerosol-radiation and  
55 indirect aerosol-cloud interactions. Aerosol optical properties can be measured directly in the laboratory  
56 and in the field using both in situ methods (Andrews et al., 2004; Moosmuller et al., 2009; Coen et al.,  
57 2013) and remote sensing instruments/platforms, such as sunphotometers and satellites (Holben et al.,  
58 1998; Anderson et al., 2005). Alternatively, aerosol optical properties can be inferred from  
59 measurements of particle composition, abundance and size distributions (Atkinson et al., 2015). One  
60 particular advantage of the remote sensing instruments is that they allow for characterization of  
61 column-average atmospheric particle burdens and properties over a large spatial scale and are free from  
62 sampling biases as the particles are characterized as they exist in the atmosphere. However, they can  
63 only reliably retrieve aerosol properties under cloud-free conditions, and determination of properties  
64 beyond the aerosol optical depth (such as the single scatter albedo or the aerosol size distribution)  
65 typically requires a data ‘inversion’ process that relies on an assessment of the wavelength-dependent  
66 light attenuation and scattering (Dubovik and King, 2000). *In situ* methods can allow for more detailed  
67 characterization of aerosols, including the relationships between size, composition and optical  
68 properties, but typically at the expense of reduced spatial coverage and with long-term measurements  
69 typically restricted to the surface (Andrews et al., 2004). Given the wide-spread use of aerosol remote  
70 sensing and the extensive availability of the data (in particular from ground-based sunphotometer  
71 networks such as AERONET and AEROCAN (Holben et al., 1998; Bokoye et al., 2001)), continued

72 assessment and validation of the inversion methods by comparison with measurements by *in situ*  
73 methods is important.

74 Multi-wavelength optical measurements can yield information about the aerosol size distribution, a  
75 principle that dates back to Ångström's observation that the wavelength-dependence of light  
76 attenuation by particles was weaker for larger particles (diameters of hundreds of nanometers to  
77 micrometers) than for smaller particles (Ångström, 1929). One of the simplest ways of characterizing the  
78 wavelength-dependence of optical measurements (whether extinction, scattering or absorption) is  
79 through the Angstrom exponent. For a pair of optical measurements at different wavelengths,  $\alpha$   
80  $= -\log(b_{x,\lambda_1}/b_{x,\lambda_2})/\log(\lambda_1/\lambda_2)$ , where  $b_{x,\lambda}$  is the optical coefficient at one of the wavelengths  $\lambda$ ; for  
81 scattering and extinction  $\alpha$  typically increases as particle size decreases. The dependence of  $b_x$  on  
82 wavelength can alternatively be obtained from a  $\log(b_{x,\lambda})$  vs.  $\log(\lambda)$  plot using two or more wavelengths;  
83 if the dependence is linear, a regression would obtain the same value as the pair-wise treatment, but  
84 non-linearity can be accommodated by using the continuous derivative  $\alpha = -d\ln(b_{x,\lambda}) / d\ln(\lambda)$  at a  
85 specified wavelength. A list of the symbols and acronyms used in this work is provided in Appendix A.  
86 The two-wavelength version will be referred to here as the Ångström exponent and the multi-  
87 wavelength variant as the spectral derivative. Particle size classification schemes have been proposed  
88 (Clarke and Kapustin, 2010) and supported/validated (Eck et al., 2008; Massoli et al., 2009; Cappa et al.,  
89 2016) based on the Ångström exponent of extinction or scattering. When observations are made at  
90 more than two wavelengths (ideally, widely spaced), further information regarding the nature of the  
91 particle size distribution can be extracted. For example, an additional level of refinement of wavelength-  
92 dependent measurements of aerosol optical depth (path integrated extinction) was introduced by  
93 O'Neill et al. (2005) to aid in the interpretation of the data obtained by the ground-based  
94 sunphotometer networks AERONET and AEROCAN. Specifically, O'Neill et al. (2003; 2005) showed that  
95 the fine mode fraction (FMF) of extinction and the fine mode effective radius,  $R_{eff,f}$  could be extracted  
96 directly from the multi-wavelength optical depth or extinction measurements available from remote  
97 sensing. The FMF provides for an approximate discrimination between what are typically naturally  
98 produced coarse mode particles (dust or sea spray) and what are often anthropogenically associated  
99 fine mode particles. Thus, parameters such as the FMF can provide a nominal indication of the relative  
100 contributions of natural versus anthropogenic particles to the atmospheric AOD. Variations in  $R_{eff,f}$   
101 provide information on the sources of the fine mode particles - as different sources yield fine mode

Deleted: (

Deleted: .)

Deleted: former

Deleted: latter

106 particles with different size distributions - or the extent to which particles have undergone atmospheric  
107 processing, which can change the size distribution (and chemical composition) in systematic ways.

108 In the spectral curvature approach of O'Neill et al. (2003), the fine mode spectral derivatives ( $\alpha_f$  = first  
109 derivative and  $\alpha_f'$  = second) and the FMF are first extracted from multi-wavelength extinction data using  
110 a process described as Spectral Deconvolution. The fine mode spectral derivatives can then be used to  
111 obtain the fine mode effective radius from a fine mode spectral curvature algorithm. Alternatively, the  
112 fine mode effective radius can be calculated from direct measurements of size distribution (e.g. from  
113 scanning mobility particle sizer) using equation 1 (Hansen and Travis, 1974):

$$114 R_{eff,f} = \frac{\int_0^{\infty} R \pi R^2 \frac{dN}{d \ln R} d \ln R}{\int_0^{\infty} \pi R^2 \frac{dN}{d \ln R} d \ln R}$$

(1)

115 where  $R$  is the particle geometrical radius and  $dN/d \ln R$  is a number weighted size distribution for which  
116  $R_{eff,f}$  is the first moment (average radius) of the surface-area weighted size distribution.  $R_{eff,f}$  is an  
117 effective radius that characterizes, approximately, the average size of particles in the fine mode that  
118 scatter solar radiation. In this work, we compare the optically obtained  $R_{eff,f}$  retrievals to those  
119 calculated by numerically evaluating the integrals of Equation 1 using the observed size distributions  
120 produced by scanning mobility particle sizers. A single log-translatable particle size distribution (i.e., a  
121 PSD that can be translated along the log-transformed particle size axis without changing the form of the  
122 distribution function) is, in many cases, a reasonable representation of the size distribution of observed  
123 aerosol fine modes (O'Neill et al., 2005). In these cases, the fine mode can be characterized by the single  
124 parameter  $R_{eff,f}$  facilitating comparisons and examination of trends in sources and/or atmospheric  
125 processing.

126 Numerical methods such as those developed by O'Neill et al. (2003) were originally applied to remote  
127 sensing measurements, but can also be applied to *in situ* extinction measurements. Beyond adding to  
128 the utility of the *in situ* optical measurements, this provides an opportunity to test the methods against  
129 other, complementary measures of particle size and size-dependent scattering and extinction. For  
130 example, Atkinson et al. (2010) used the approach of O'Neill et al. (2003) to analyze *in situ*, three-  
131 wavelength aerosol extinction measurements made during the 2006 TexAQs II campaign near Houston,  
132 TX. More recently, Kaku et al. (2014) showed, for a range of marine atmospheres, that the application of  
133 this spectral approach to obtain FMF from three-wavelength scattering coefficient measurements was  
134 largely coherent with the sub-micron fraction of scattering (SMF), obtained from scattering coefficient  
135 measurements of the fine and coarse mode components using impactor-based separation of the

Deleted: ( $\eta$  was used for FMF in *ibid.*) The fine mode spectral derivatives are then used to obtain the effective radius for the fine mode, defined by Hansen and Travis (1974) as:

Deleted: (1)

Deleted: from

Deleted: (

Deleted: ) by numerically evaluating the integrals of Equation 1 to produce comparator values

Deleted: Methods

Deleted: for

147 aerosol. These studies, and others, provide a useful basis for understanding the accuracy and  
148 applicability of the parameters retrieved from remote sensing data. However, further assessment in a  
149 wide range of environments is necessary given that networks employing such spectral remote sensing  
150 algorithms (AERONET and some surface based sites) represent locations impacted by particles from  
151 diverse sources.

152 In this work, measurements of aerosol optical properties (extinction, scattering and absorption  
153 coefficients) made at multiple wavelengths during the 2010 Carbonaceous Aerosols and Radiative  
154 Effects Study (Fast et al., 2012; Zaveri et al., 2012) are reported and analyzed using the O'Neill et al.  
155 (2003) and the O'Neill et al. (2008b) methods. The measurements were made at two locations near  
156 Sacramento: a more urban site in Granite Bay, CA (T0) and a more rural site in Cool, CA (T1) that were  
157 often linked by direct atmospheric transport. The multi-wavelength measurements were made using  
158 three types of optical instruments (specifically seven separate instruments at the two locations). The  
159 multi-wavelength measurements of the extinction coefficients (either measured directly or produced  
160 from the sum of scattering and absorption coefficients) are used to retrieve the fine mode fraction of  
161 extinction and fine mode effective radius. These results from the retrieval, described in more detail in  
162 the next section, are compared to other, complementary *in situ* measurements. Scattering and  
163 absorption coefficients were measured after aerodynamic separation into the PM<sub>1</sub> and PM<sub>10</sub> fractions,  
164 which allowed the sub-micron fraction (SMF) of extinction to be directly determined. The *in situ* SMF can  
165 be compared with the FMF from the spectral retrieval method. In this work, sub-micron particles are  
166 those with nominal aerodynamic diameters ( $d_{p,a}$ ) smaller than 1  $\mu\text{m}$ , likely resulting in geometric  
167 diameters below 800 nm. Also, size distribution measurements allowed for determination of the fine-  
168 mode effective radii (via Eqn. 1), which are compared with those obtained from the spectral retrieval.

Deleted: (

Deleted: .)

Deleted: that

## 169 Theoretical Approach

### 170 *The Spectral Deconvolution Algorithm with Fine Mode Curvature (SDA-FMC) Approach*

Formatted: Font: (Default) +Body (Calibri), 12 pt, Not Bold, Italic, Font color: Custom Color(RGB(34,34,34))

171 This section provides a qualitative description of the fine and coarse mode AOD (or extinction) retrieval  
172 algorithm (SDA, or spectral deconvolution algorithm) and fine mode optical sizing (FMC or fine mode  
173 curvature) method developed by O'Neill. The details of the derivation and application of the SDA are  
174 provided in previous publications (O'Neill et al., 2003; Atkinson et al., 2010; Kaku et al., 2014). The  
175 MATLAB code that implements the approach is available from O'Neill upon request. Application of both  
176 approaches requires a robust set of measurements of aerosol optical extinction or scattering (or optical

Deleted: (SDA)

Deleted: 2005

182 depth) at a minimum of three wavelengths that should be widely spread across the optical region of the  
183 spectrum (near UV through the visible to the near IR; see, for example, O'Neill et al. (2008a)).

184 The fundamental assumption of the SDA approach is that most ambient aerosol size distributions are  
185 composed of two optically-relevant modes: a fine mode having an effective radius (and to a lesser  
186 extent, geometric standard deviation) that is a function of atmospheric processing, and a separate  
187 coarse mode, largely in the supermicron ( $d_{p,a} > 1 \mu\text{m}$ ) size range. A common assumption is that the fine  
188 mode is more closely associated with anthropogenic activities and the coarse mode with natural  
189 sources, although this can be somewhat confounded by smoke from biomass burning (Hamill et al.,  
190 2016). In particular, it can be difficult to distinguish biomass burning particles from particles derived  
191 from urban sources, as both primarily fall within the fine mode and are somewhat absorbing. The FMC  
192 (Fine Mode Curvature) algorithm employs the fine mode optical parameters retrieved using the SDA to  
193 estimate both a fundamental indicator of optical particle size (the fine mode van de Hulst parameter)  
194 and from this, an indicator of microphysical particle size (the fine mode effective radius); these are both  
195 defined below.

#### 196 ***Spectral deconvolution of the fine and coarse mode extinction and derivation of the fine mode*** 197 ***spectral derivatives (SDA)***

198 The spectral deconvolution algorithm begins by isolating the fraction of total extinction due to particles  
199 in the fine mode, based on the stronger dependence of the extinction (scattering)<sup>1</sup> on wavelength for  
200 smaller particles. Current applications of the method start by fitting  $\ln(b_{\text{ext}})$  (or  $\ln(b_{\text{scat}})$  or  $\ln(\text{AOD})$ )  
201 versus  $\ln(\lambda)$  to a second order polynomial, where  $b_{\text{ext}}$  is the measured wavelength-dependent extinction  
202 coefficient (see Atkinson et al. (2010) and Kaku et al. (2014) for scattering and extinction coefficient  
203 applications, Saha et al. (2010) for a sunphotometry AOD application and Baibakov et al. (2015) for a  
204 starphotometry AOD application). The extinction and its first and second derivatives are determined  
205 from the fit at a reference wavelength of 500 nm, a common reference wavelength along with 550 nm  
206 in optical studies. The first derivative (i.e. slope) is denoted  $\alpha$  in analogy to the Ångström exponent, but  
207 in this non-linear, second order approach it is a function of wavelength. The second derivative  $\alpha'$  (i.e.  
208 spectral curvature) may, in principle, be wavelength dependent over the observed range, but using a  
209 second order polynomial fit yields a constant value. Values of  $\alpha$  and  $\alpha'$  associated with the fine mode

**Deleted:** are determined from the fit

**Deleted:** wavelength-invariant version.

<sup>1</sup> We will stop inserting “(scattering)” at this point although all references below should be understood to apply to both scattering and extinction.

212 and the coarse mode are indicated using subscript f or c, respectively. In this work, only a second order  
 213 fit is possible because only three measurements are used to define the wavelength dependence. In the  
 214 SDA-FMC approach, the observed spectral derivative ( $\alpha$ ) is used along with the SDA-derived fine mode  
 215 spectral derivative ( $\alpha_f$ ) to produce the fine mode fraction of extinction (FMF), given as:

$$217 \quad FMF = \frac{\alpha - \alpha_c}{\alpha_f + \alpha_c} \quad (2)$$

218  
 219 Ultimately, the fine mode slope and curvature are both used in the FMC algorithm to determine the fine  
 220 mode effective radius (discussed in the next section).

221 The algorithm proscribes constant values of the spectral slope and curvature for all coarse mode  
 222 aerosols ( $\alpha_c$  and  $\alpha'_c$ ) at the reference wavelength of 500 nm. Specifically,  $\alpha_c = -0.15 \pm 0.15$  and  $\alpha'_c =$   
 223  $0.0 \pm 0.15$ , with the uncertainties as per O'Neill et al. (2003), O'Neill et al. (2001) showed that an  
 224 assumption of an aerosol size distribution with two distinct modes yields a series of three equations that  
 225 express the relationships between the observed parameters (AOD or extinction coefficient,  $\alpha$ ,  $\alpha'$ ) and  
 226 their fine and coarse mode analogues. Specifically, the equations can be inverted to yield the fine mode  
 227 spectral derivative, the fine mode curvature ( $\alpha'_f$ ) and the fine and coarse mode AOD or  $b_{ext}$  values. It  
 228 should be noted that the fitting of a 2<sup>nd</sup> order polynomial to input AOD or  $b_{ext}$  spectra is only an  
 229 approximation relative to a higher order polynomial. The use of a 2<sup>nd</sup> order polynomial represents a  
 230 compromise between higher order spectral polynomials being better representations of theoretical Mie  
 231 spectra and the beneficial damping effects of lower order polynomials in the presence of noisy spectra  
 232 (O'Neill et al., 2001). The observationally determined total and fine mode spectral derivative and  
 233 proscribed coarse mode spectral derivative are then used to calculate the fine mode fraction of  
 234 extinction at the reference wavelength (here 500 nm) using Eqn. 2.

236 **Estimation of the Fine Mode Effective Radius – the Fine Mode Curvature (FMC) approach**

237 Using the SDA-derived, fine mode spectral derivatives ( $\alpha'_f$  and  $\alpha_f$ ), an estimate of the fine mode  
 238 effective radius is obtained. The basis for this approach is a fundamental parameterization involving the  
 239 effective van de Hulst phase shift parameter for fine mode aerosols and its representation in  $\alpha'_f$  versus

**Deleted:** combined

**Deleted:** of the fine modes

**Deleted:** while the fine mode slope and curvature are both used in determining the fine mode effective radius.

**Formatted:** Font: 12 pt, Italic

**Deleted:** One reason for choosing a mid-visible reference wavelength of 500 nm for assessing curvature and slopes is that the variation of the extinction for coarse mode aerosols is minimal in this spectral region (O'Neill et al., 2001). The algorithm assumes constant values of the spectral slope and curvature for all coarse mode aerosols at this wavelength (500 nm), specifically  $\alpha_c = -0.15$  and  $\alpha'_c = 0.0$  (with an assumed uncertainty, as per

**Formatted:** Left

**Deleted:** , of  $\pm 0.15$  and  $\pm 0.15$  respectively). An

**Deleted:** aerosol bimodality (at least as far as measurements in the visible and near-IR are concerned)

**Deleted:** succinct

**Deleted:** if the approximation level relative to a theoretical Mie representation (O'Neill et al., 2001) is limited to second order in  $\ln \lambda$  space. These three equations

**Deleted:** (O'Neill et al., 2001). A set of three

**Deleted:** then

**Deleted:** as:¶

**Deleted:** Using the spectral derivatives for the fine mode obtained from the SDA portion of the approach, an estimate of the fine mode effective radius is obtained. The basis for this approach is a parameterization of a strong relationship between the effective van de Hulst phase shift parameter for fine mode aerosols and a polar angle representation of  $\alpha'_f$  vs.  $\alpha_f$  (O'Neill et al., 2005). The fundamental van de Hulst parameter for the fine mode,  $\rho_{eff,f}$ , is given by:¶

271  $\alpha_f$  space. Full details are provided in O'Neill et al. (2005) and O'Neill et al. (2008b), and only a summary  
272 of the parameterization is provided here. The van de Hulst parameter for the fine mode,  $\rho_{eff,f}$ , is given  
273 by:

$$274 \rho_{eff,f} = 2 * \frac{2 \pi R_{eff,f}}{\lambda} |m - 1|$$

(3)

275  
276 where  $\lambda$  is the reference wavelength and  $m$  is the complex refractive index at that wavelength (O'Neill et  
277 al., 2005). An estimate of this purely optical parameter is based on a 3<sup>rd</sup> order polynomial derived from  
278 numerical Mie simulations that relate  $\rho_{eff,f}$  and the polar angle ( $\psi$ ) coordinate of any point in  $\alpha_f'$  vs.  $\alpha_f$   
279 space (O'Neill et al., 2005). The value of  $\psi$  for any given retrieval is simply the arctangent of  $\alpha_f'$  divided  
280 by  $\alpha_f$  (minus small prescribed offsets of  $\alpha_{f,0}'$  over  $\alpha_{f,0}$  respectively). Individual simulated contour curves  
281 of  $\alpha_f'$  versus  $\alpha_f$  correspond to particle size distributions of differing  $R_{eff,f}$  for constant values of refractive  
282 index and were illustrated in Figure 1 of O'Neill et al. (2005). The three different "lines of constant  $\rho_{eff,f}$ "  
283 in that figure correspond to three different values of  $\psi$  (where both  $\rho_{eff,f}$  and  $\psi$  increase in the  
284 counterclockwise direction from the horizontal). The  $R_{eff,f}$  value are then computed from the retrieved  
285 value of  $\rho_{eff,f}$ , by inverting equation (3), if the refractive index of the particles is known. Since the  
286 refractive index is generally unknown for the situations we consider here, the information provided by  
287 this approach is actually a combination of size and composition. In many cases, an average, constant  
288 value for the real portion of the refractive index can be assumed and the imaginary part neglected to  
289 provide an estimate of the effective radius; this is, in part, because the imaginary component is typically  
290 much smaller than the real component of the refractive index, and thus the  $R_{eff,f}$  value is relatively  
291 insensitive to variations in the imaginary component. This treatment is questionable if strong changes in  
292 the average composition that lead to changes in  $m$  are suspected. For example if the composition  
293 shifted from pure sulfate aerosol ( $m = 1.53 + 0i$ ) to a brown carbon organic ( $m = 1.4 + 0.03i$ ) this would  
294 introduce a 33% shift in the derived radius with no change in actual size; the majority of this shift in the  
295 derived radius results from the change in the real component of the refractive index.

296 The FMC method represented by the inversion of equation (3) has been less rigorously validated than  
297 the SDA portion and is expected to be more susceptible to problems related to measurement errors and  
298 a decreasing sensitivity with decreasing fine mode fraction of extinction. The FMC validation is largely  
299 confined to comparisons with the more comprehensive AERONET inversions of Dubovik and King (2000),  
300 referred to henceforth as the D&K inversions. These inversions, which require the combination of AOD  
301 and sky radiance data, are of a significantly lower frequency than simple AOD measurements. The sky

Deleted: (3)

Formatted: Left, Line spacing: Multiple 1.08 li

Deleted: ¶

where  $\lambda$  is the reference wavelength and  $m$  is the complex refractive index at that wavelength (ibid.) An estimate of this purely optical parameter derived from the  $\alpha_f'$  vs.  $\alpha_f$  polar relationship allows extraction of an effective radius for the fine mode from the SDA-obtained slope and curvature, if the refractive index of the particles is known.

Formatted: Default Paragraph Font, Font: Calibri, Font color: Auto, Pattern: Clear

Deleted:  $\rho_{eff}$

Formatted: Default Paragraph Font, Font: Calibri, Font color: Auto, Not Superscript/ Subscript, Pattern: Clear

Formatted: Default Paragraph Font, Font: Calibri, Font color: Auto, Subscript, Pattern: Clear

Formatted: Default Paragraph Font, Font: Calibri, Font color: Auto, Pattern: Clear

Deleted: , for

Formatted: Default Paragraph Font, Font: Calibri, Font color: Auto, Pattern: Clear

Deleted: would result

Formatted: Default Paragraph Font, Font: Calibri, Font color: Auto, Pattern: Clear

Deleted: The FMC method has been less rigorously validated than the SDA portion and is expected to be more susceptible to problems related to measurement errors and a decreasing sensitivity with decreasing fine mode fraction of extinction. The polar-coordinate system relationship is a strong, near monotonic fit based on Mie simulations over a variety of aerosol types and sizes (O'Neill et al., 2005; O'Neill et al., 2008a); its validation is largely confined to comparisons with the more comprehensive AERONET inversions of (Dubovik and King, 2000). These inversions, which require the combination of AOD and sky radiance data, are of a significantly lower frequency than simple AOD measurements (nominally once per hour versus once every 3 minutes respectively). The comparisons (for the limited data set of O'Neill et al. (2005) and confirmed by more recently unpublished AERONET-wide comparisons) show averaged AERONET-SDA differences of  $10\% \pm 30\%$  for large FMF values  $> 0.5$ .

331 radiance data are collected nominally once per hour while AOD measurements are made once every 3  
332 minutes. Comparisons between the FMC method and the D&K inversions show averaged FMC versus  
333 AERONET differences of  $10\% \pm 30\%$  (mean  $\pm$  standard deviation of  $(\rho_{\text{eff},f,\text{FMC}} - \rho_{\text{eff},f,\text{D\&K}}) / \rho_{\text{eff},f,\text{D\&K}}$ ) for  
334 large FMF values  $> 0.5$ , at least for the limited data set of O'Neill et al. (2005) and confirmed by more  
335 recently unpublished AERONET-wide comparisons between the FMC and D&K methods.

### 336 **Application of the SDA-FMC method to in situ extinction measurements**

337 This paper seeks to address the following two key questions pertaining to the use of the SDA-FMC  
338 algorithm with extinction measurements, especially those produced by the cavity ring-down  
339 instruments, to extract information about aerosol size, both the partitioning of the extinction between  
340 the fine and coarse modes and the extraction of a single parameter size characterization of the fine  
341 mode.

342 1.) Can the approach be used reliably to extract the fine and coarse mode fractions of the  
343 extinction in situations where only a single optical instrument is used?

344 and,

345 2.) In situations where complementary measurements (mobility-based sizers, parallel or switching  
346 nephelometers, etc.) are available, what information can be determined from the comparison of  
347 the products of the SDA-FMC approach to comparable information obtained in other ways?

348 It has been suggested that a single multi-wavelength optical measurement of the fine mode fraction  
349 could be less expensive than derivation of the sub-micron fraction of scattering using parallel  
350 nephelometers (Kaku et al., 2014). The use of two size-selected inlets (e.g., 1 and 10  $\mu\text{m}$  cyclones) and  
351 parallel nephelometers is not prohibitively expensive, but the typical concerns regarding calibration  
352 maintenance and careful and consistent application of correction factors for truncation angle and non-  
353 Lambertian illumination can be magnified when measurements are combined (either as differences or  
354 ratios) since systematic errors may not undergo partial cancellation like random errors.

355 In principle, the use of two parallel CRD extinction measurements could mitigate some of the possible  
356 errors with parallel nephelometers. Cavity ring-down measurements directly quantify total extinction  
357 within the cavity, which is contributed from both gases and particles (Smith and Atkinson, 2001; Brown,  
358 2003). To determine extinction by aerosols only, the entering air stream is periodically directed through  
359 a filter such that a gas-only reference is determined. Extinction by aerosol particles is determined

**Deleted:** do not (in principle) need to be calibrated and have very small truncation errors

**Deleted:** In practice, two types of "calibrations" are applied to CRD measurements: a zeroing procedure

**Deleted:** is usually

**Deleted:** measurement of filtered air for

**Deleted:** measurements and a cavity path length correction because

368 [relative to this gas zero. The aerosol extinction is further corrected to account for the practical aspect](#)  
369 [that](#) the complete mirror-to-mirror distance of the optical cavity is typically not filled with aerosols (to  
370 keep the mirrors clean) (Langridge et al., 2011). The former (zeroing) limits instrument precision and  
371 sometimes accuracy while the latter (path length) limits instrument accuracy. In general these  
372 procedures are identical for the two parallel instruments and are very stable in time, so they would only  
373 be expected to produce a small and consistent bias. To our knowledge, currently no single-package,  
374 multi-wavelength direct extinction (cavity-enhanced) instruments are commercially available. Multiple  
375 single-wavelength instruments operating at different wavelengths could be deployed, but might be  
376 prohibitively expensive.

377 For detailed knowledge of the fine mode size distribution, the use of scanning mobility analyzer-based  
378 sizing instruments is preferable since the full mobility size distribution is obtained, as opposed to only  
379 the effective radius provided by the FMC procedure. However, scanning mobility sizer instruments  
380 typically have maximum diameters of only 700 to 800 nm, and both scanning and multi-channel variants  
381 are of comparable expense and complexity as CRD instruments. In order to obtain additional  
382 information about the coarse mode size distribution and contribution to the optical effects, an aerosol  
383 particle spectrometer (APS) is generally added to the measurement suite.

384 The purely spectrally-based mode separation inherent in the SDA obviates the need for a physical cut  
385 point selection, such as that required to measure the PM<sub>1</sub> scattering product used in this work. This can  
386 be advantageous, since selection and maintenance of a size cut-point is a possible source of differences  
387 between some measurements (and variability of all measurements using physical separation) of the sub-  
388 micron fraction (SMF) of scattering, absorption or extinction. The SMF is fundamentally different from  
389 the FMF, although both provide an indication of the fractional optical contribution of smaller particles.  
390 In fact, there are fundamental differences between many of the SMF or FMF data products that are  
391 currently available. For example, the Dubovik and King (2000) SMF data product tries to locate the  
392 separation radius (called the inflection point) at a minimum of the particle size distribution obtained  
393 from the inversion procedure. This results in a variable cut point that can be interpreted as assigning a  
394 portion of the coarse mode to the fine mode (O'Neill et al., 2003). The aerodynamic diameter selected  
395 for the physical separation used in the SMF presented in this work might result in some mis-assignment  
396 of fine mode extinction to the coarse mode, since (i) the aerodynamic separation results in a cut point  
397 that is less than 1  $\mu\text{m}$  geometric diameter and (ii) the cut point might not correspond to a local  
398 minimum of the size distribution. These definitional differences should be kept in mind when comparing

399 fine mode apportionments (SMF or FMF) from different measurements/data treatments. And all of  
 400 these data products will usually differ significantly from the optical properties of the PM<sub>2.5</sub> fraction used  
 401 to define the fine mode for air quality regulations and to exclude larger particles in the CRD instruments  
 402 at T0. The latter allowed a significant fraction, but not all of the optically coarse particles into the  
 403 instruments, as shown in the Results section. For the comparisons presented in this work, in cases  
 404 where there is significant penetration of one of the modes into the size regime defined by the physical  
 405 cut-point as the other mode (or significant overlap of two or more size modes) there are noticeable  
 406 differences between the physically-defined SMF and the FMF produced by the SDA.

## 407 Experimental

408 The instrument suites used, sampling conditions and methodology and goals of the CARES study have  
 409 been summarized by Zaveri et al. (2012). A summary of the instrumentation used to make the light  
 410 extinction, scattering and absorption measurements is provided in Table 1. Extinction was measured  
 411 either directly (using cavity ringdown spectroscopy) or as the sum of scattering and absorption. A brief  
 412 description of the key instruments used in the current analyses is given below.

413

414 **Table 1: Summary of optical instruments used at the T0 and T1 sites**

Property	Instrument	Wavelength	Size Cut*
<i>T0</i>			
Extinction	UCD CRD	405, 532 nm	2.5 μm
	PSU CRD	532, 1064 nm	2.5 μm
Scattering	PNNL Nephelometer	450, 550, 700 nm	1 μm, 10 μm
Absorption	PNNL PSAP	470, 522, 660 nm	1 μm, 10 μm
<i>T1</i>			
Extinction	PSU CRD	355, 532, 1064 nm	None applied
Scattering	PNNL Nephelometer	450, 550, 700 nm	1 μm, 10 μm
Absorption	PNNL PSAP	470, 522, 660 nm	1 μm, 10 μm

\*For the entries with two size cuts listed, the sampling system switched between the two on a 6 minute cycle

415

### 416 ***Instruments used at the T0 site (American River College, Granite Bay, CA USA)***

417 Cavity Ring-down Extinction: The  $b_{ext}$  measurements at 405 nm and 532 nm were made using the UC  
 418 Davis two-wavelength Cavity Ring Down-Photoacoustic Spectrometer (CRD-PAS) instrument (Langridge  
 419 et al., 2011; Lack et al., 2012). Full details of these measurements are available in Cappa et al. (2016) and  
 420 Atkinson et al. (2015). These measurements were only made for a subset of the CARES campaign, from

Deleted: (

Deleted: .,

423 20:00 PDT on 16 June through 09:00 PDT on 29 June. At 532 nm,  $b_{ext}$  was measured at low (~25%), mid  
424 (~75%) and high (~85%) relative humidity. At 405 nm only low RH measurements were made, and so  
425 only the low RH 532 nm measurements are used in this study. The CRD-PAS sampled behind a PM<sub>2.5</sub>  
426 (aerodynamic diameter <2.5 μm) URG Teflon-coated aluminum cyclone. A separate CRD instrument  
427 deployed by the PSU group at T0 used a single optical cavity to measure the sub-2.5 μm (sampled  
428 through a similar URG cyclone) aerosol extinction coefficient at 532 and 1064 nm simultaneously  
429 (Radney et al., 2009). This instrument did not incorporate intentional RH control, but efforts were made  
430 to maintain nearly ambient conditions, resulting in low RH (25 - 40 %) throughout most of the campaign,  
431 as measured by an integrated RH/T sensor (Vaisala HMP70). Daytime ambient RH was similar to the low  
432 RH value during the CARES campaign (Fast et al., 2012).

433 ~~To obtain three-wavelength  $b_{ext}$  measurements for use in the SDA-FMC analysis, we combined the~~  
434 ~~measurements from the two CRD instruments, (the 1064 nm measurements from the PSU instrument~~  
435 ~~were used with the 532 nm and 405 nm UCD data after all had been averaged to one-hour). To assess~~  
436 ~~whether this was a reasonable approach, the 532 nm time series data from the two instruments were~~  
437 ~~overlaid and examined for differences. There is a high degree of temporal correspondence between the~~  
438 ~~measurements from the two instruments, although there was a clear difference in precision, with the~~  
439 ~~UCD CRD having approximately 3 times better precision than the PSU instrument at comparable~~  
440 ~~integration times. This difference in precision results from differences in instrumental design and (likely)~~  
441 ~~mirror quality. A scatterplot (Figure S1) of  $b_{ext,PSU}$  versus  $b_{ext,UCD}$  also showed good correlation, with a~~  
442 ~~best fit line from an orthogonal distance regression fit having a slope = 0.96 and an intercept that was~~  
443 ~~statistically indistinguishable from zero. This is within the uncertainties of the instruments. The good~~  
444 ~~agreement at 532 nm between the PSU and UCD instruments suggests that combining the 1064 nm~~  
445 ~~measurements from PSU with the 405 nm and 532 nm measurements from UCD is reasonable. If the~~  
446 ~~very slight low bias in the 532 nm  $b_{ext}$  from PSU relative to the UCD measurements applies to the 1064~~  
447 ~~nm measurements then the derived FMF values might be slightly overestimated.~~

448 Size-selected absorption and scattering (nephelometer and PSAP): The low RH scattering and absorption  
449 coefficients were alternatingly measured for PM<sub>10</sub> and PM<sub>1</sub> aerodynamic size selected aerosol using the  
450 PNNL Aerosol Monitoring System, a clone of NOAA/CMDL's Aerosol Monitoring System (detailed  
451 description at <http://www.esrl.noaa.gov/gmd/aero/instrumentation/instrum.html> and in Zaveri et al.  
452 (2012)). The relevant measurements are: light absorption coefficients at three-wavelengths (Radiance  
453 Research Particle Soot Absorption Photometer [PSAP]) and total scattering coefficients (three-

Formatted: Font: +Body (Calibri)

Formatted: Font: +Body (Calibri)

Formatted: Font: +Body (Calibri)

Deleted: . First

Formatted: Font: +Body (Calibri)

Formatted: Font: +Body (Calibri)

Deleted: :

Formatted: Font: +Body (Calibri)

Deleted: data was demonstrated (except for

Formatted: Font: +Body (Calibri)

Formatted: Font: +Body (Calibri)

Deleted: ).

Formatted: Font: +Body (Calibri)

Deleted: between the two data sets

Formatted: Font: +Body (Calibri)

Formatted: Font: +Body (Calibri)

Formatted: Font: +Body (Calibri)

Deleted: 87

Formatted: Font: +Body (Calibri)

Deleted: With this assurance

Formatted: Font: +Body (Calibri)

Deleted: the two instruments were measuring the same aerosol with comparable measurement quality, the PSU 1064 nm data are used with the UCD 532 nm and 405 nm

Formatted: Font: +Body (Calibri)

Deleted: RH data for the SDA-FMC analysis

Formatted: Font: +Body (Calibri)

Deleted: Nephelometer

467 wavelength nephelometer, TSI 3563). The scattering coefficients were corrected for truncation error  
468 (Anderson and Ogren, 1998) and the absorption coefficients for filter effects (Ogren, 2010). The  
469 absorption coefficients were interpolated to the nephelometer wavelengths assuming the inverse  
470 wavelength dependence characteristic of uncoated black carbon, as appropriate for this region (Cappa  
471 et al., 2016). The absorption and scattering coefficients for PM<sub>1</sub> or PM<sub>10</sub> are then summed after  
472 averaging to one-hour intervals and using the mean of the 450 and 550 nm values to obtain b<sub>ext</sub>(500  
473 nm). The extinction fraction of the PM<sub>1</sub> (herein, the SMF) at the visible wavelength (500 nm) is then  
474 calculated from their ratio

$$475 \text{SMF}_{ext} = \frac{b_{ext,PM1}}{b_{ext,PM10}}$$

(4)

476 Particle size control was effected by 2 impactors (1 μm and 10 μm) upstream of the PSAP and  
477 nephelometer. The 10- μm impactor was always present in the sampling line, and the flow was switched  
478 to run through the 1- μm impactor on 6-min intervals, yielding alternating 6-min measurements of  
479 submicron and coarse (< 10 μm) particle modes.

480 Fine particle size distribution: The submicron dry particle mobility diameter ( $d_{p,m}$ ) size distribution (12  
481 nm to 737 nm) was measured using a scanning mobility particle sizer (SMPS) comprised of a charge  
482 neutralizer, differential mobility analyzer and condensation particle counter (TSI 3081 DMA column and  
483 model 3775 CPC). The SMPS data were corrected for multiply-charged particles and diffusional losses.  
484 These size distribution measurements are used to calculate  $R_{eff,f}$  values from Eqn. 1, which will be  
485 referred to as  $R_{eff,f,size}$ . It should be noted that a mobility diameter of 737 nm corresponds to an  
486 aerodynamic diameter of 919 nm (assuming a density of 1.5 g cm<sup>-3</sup>, a reasonable value for the campaign  
487 based on the observed particle composition (Atkinson et al., 2015)).

488

## 489 ***Instruments used at the T1 site (Evergreen School, Cool, CA USA)***

490 Cavity Ring-down Extinction: The PSU group deployed a custom CRD instrument that used separate  
491 optical cavities to measure  $b_{ext}$  at 355 nm, 532 nm, and 1064 nm simultaneously in each of four separate  
492 flow systems that were intended to measure total and submicron aerosol and submicron aerosol that  
493 had been conditioned to have elevated and suppressed RH. Only the total aerosol flow results are used  
494 here as this prototype system suffered from signal to noise problems and RH/temperature control  
495 issues. As with the T0 PSU instrument, the total aerosol system attempts to measure particle extinction

**Deleted:** The absorption coefficients were adjusted to the nephelometer wavelengths using an inverse wavelength dependence.

**Deleted:** (4)

**Deleted:** Nephelometer

**Formatted:** Heading 2, Line spacing: single

501 at nearly ambient conditions, resulting in low RH (25 – 40 %) throughout most of the campaign, as  
502 measured by an integrated RH/T sensor (Vaisala HMP70). No intentional size cut was applied to these  
503 measurements, although the system was not optimized for transmission of coarse mode particles.

504 Size-selected absorption and scattering (Nephelometer and PSAP): An identical instrument suite to that  
505 used at T0 was deployed and the same data analysis was conducted.

506 Fine particle size distribution: The SMPS used at T1 is a similar design described in (Setyan et al., 2012)  
507 and it measured low RH particle sizes from 10 nm to 858 nm. The SMPS data were corrected to take into  
508 account the DMA transfer function, the bipolar charge distribution, the CPC efficiency and the internal  
509 diffusion losses (Setyan et al., 2014).

Deleted: .

#### 510 **Uncertainties in the derived and measured values**

511 The uncertainty in the SMF has been estimated from standard error propagation of the uncertainties in  
512 the  $PM_{1}$  and  $PM_{10}$  extinction measurements. The assumed uncertainties in  $b_{ext,PM1}$  and  $b_{ext,PM10}$  are  $\pm 1$   
513  $Mm^{-1}$ . This uncertainty estimate accounts only for random errors, not systematic errors.

514 Uncertainties in the FMF have been estimated based on the uncertainties in the inputs to the SDA-FMC  
515 procedure, namely the  $b_{ext}$  values. The assumed uncertainties in the input  $b_{ext}$  were instrument specific:  
516  $<1 Mm^{-1}$  for the UCD CRD,  $1 Mm^{-1}$  for the nephelometer plus PSAP and PSU CRD at T0, and  $3 Mm^{-1}$  for  
517 the PSU CRD at T1. The input uncertainties are propagated through the various mathematical  
518 relationships using standard methods. The FMF error estimate includes some of the factors that  
519 contribute systematic uncertainty in the method. As noted in the Theoretical Approach section, FMF  
520 values from the SDA-FMC procedure have been shown to agree well with those determined from the  
521 more comprehensive inversion method of Dubovik and King (2000).

522 Uncertainties in the derived  $R_{eff,f}$  are also estimated from the uncertainties in the input values. The size-  
523 distribution derived  $R_{eff,f}$  values depend on the SMPS measurements. The SMPS instruments were  
524 calibrated (using 200 nm polystyrene latex spheres) prior to the campaign and a drier was used to keep  
525 the aerosol RH  $< 30\%$  throughout the entire campaign. Periodic checks throughout the campaign  
526 indicate consistent sizing performance to within 5%. The size distribution data used here were corrected  
527 for DMA transfer function, the bipolar charge distribution, the CPC efficiency and internal diffusion  
528 losses. Under these conditions the estimated uncertainties for  $D_p$  are around 10% for the size range  
529 between 20 and 200 nm (Wiedensohler et al., 2012). Although larger uncertainties could exist for  
530 smaller and larger particle sizes, the derived  $R_{eff,f}$  values fell primarily in this range. The estimated SMPS

532 uncertainty (Wiedensohler et al., 2012) was estimated based on intercomparisons between different  
533 SMPS instruments and thus probably represents both determinate and indeterminate errors. The  
534 relative uncertainty in the  $R_{eff}$  from the size distribution measurement is thus estimated to be 10%.  
535 This estimate mainly reflects uncertainties in the absolute size, since there is expected to be significant  
536 cancellation in the errors produced by the particle counter (the same data are used in the numerator  
537 and denominator of Eq. 1).  
538 Estimating the uncertainty in the  $R_{eff}$  from the SDA-FMC is more challenging because the uncertainties  
539 cannot be simply propagated through the equations. Therefore, an approach was taken wherein a large  
540 number of  $R_{eff}$  values were calculated from input  $b_{ext}$  that were independently, randomly varied within  
541 one standard deviation of the measured value, assuming a normal distribution of errors. Potential  
542 uncertainty or variability in the real refractive index was accounted for based on the compositional  
543 variation (Atkinson et al., 2015) and assuming volume mixing applies. The standard deviation (1s) was  
544 0.015. This is likely a lower estimate of the uncertainty in the RI, as it does not account for absolute  
545 uncertainty in the estimate. The standard deviation of the derived  $R_{eff}$  is taken as the uncertainty. This  
546 Monte Carlo-style approach does not incorporate systematic error sources. The relative uncertainty in  
547 the derived  $R_{eff}$  is found to range from a few percent up to 40%, depending on the particular  
548 instrument suite considered and measurement period. In general, the uncertainties were larger for the  
549 PSAP and nephelometer, presumably because the wavelengths used are more closely spaced.

550

## 551 **Results and Discussion**

### 552 ***Fine mode fraction of extinction***

553 The CRD-based extinction measurements were used to derive the  $FMF_{ext}$  using the SDA. This will be  
554 referred to as the  $FMF_{ext,CRD}$ . For the T0 site, the  $FMF_{ext,CRD}$  is for  $PM_{2.5}$  while at T1 no physical cut point  
555 was introduced, so  $PM_{10}$  is a reasonable expectation. The time series of the CRD-based  $b_{ext}$  values and of  
556 the derived  $FMF_{ext,CRD}$  at the T0 site are shown in Figure 1 (all times in PDT – local time during the study).

557 The  $FMF_{ext,CRD}$  varies from 0.54 to 0.97, with a mean of  $0.79 \pm 0.1$  (1  $\sigma$ ) as summarized in Table 2.

558

559

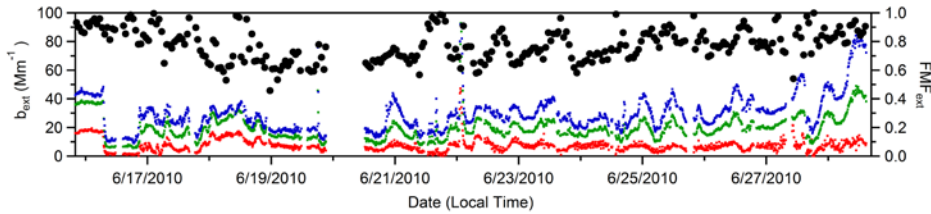
Formatted: Line spacing: Multiple 1.08 li

Deleted: 55

Deleted: 1

Deleted: 78

Deleted: ).



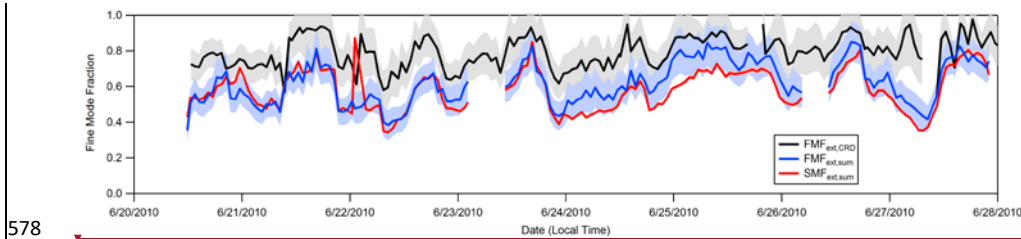
564

565 **Figure 1** – Time series of CRD extinction coefficient observations (left axis) and the derived  $FMF_{ext,CRD}$   
 566 (right axis) at T0 during the time period analyzed in this work. The blue, green and red traces are the  
 567 405 nm, 532 nm and 1064 nm  $b_{ext}$  (respectively) and the black points show the 1 h average  $FMF_{ext,CRD}$   
 568 from the SDA analysis. A  $PM_{2.5}$  size cut was applied during the sampling.

569

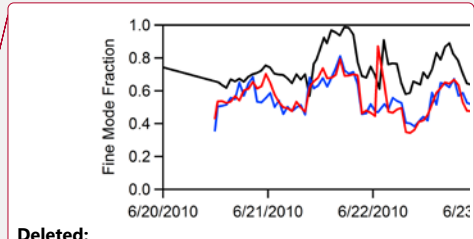
570 The fine mode fraction of extinction at T0 was alternatively determined from the  $PM_{10}$   $b_{ext}$   
 571 measurements from the nephelometer and PSAP, referred to as  $FMF_{ext,sum}$ . The SDA-derived  $FMF_{ext,CRD}$   
 572 and  $FMF_{ext,sum}$  values are compared with the sub-micron fraction of extinction determined from the  
 573 combined  $PM_1$  and  $PM_{10}$  nephelometer and PSAP measurements (from the latter part of the campaign)  
 574 at T0 (Fig. 2). The  $FMF_{ext,CRD}$ ,  $FMF_{ext,sum}$  and  $SMF_{ext,sum}$  all exhibit the same general temporal dependence.  
 575 In general, the  $FMF_{ext,CRD} > FMF_{ext,sum} \sim SMF_{ext,sum}$  although the specific relationships vary with time. For  
 576 example, there are periods when the  $FMF_{ext,sum}$  and  $SMF_{ext,sum}$  are nearly identical (e.g. 20 June – 23  
 577 June) and periods when the  $SMF_{ext,sum}$  is somewhat lower than the  $FMF_{ext,sum}$  (e.g. 24 June – 25 June).

Formatted: Right: 0.06", Line spacing: single



578

579 **Figure 2** – Time series of the fine mode fractions and sub-micron fraction of extinction at T0. The  
 580 red trace is the  $SMF_{ext,sum}$  determined from the  $b_{ext}(PM_1) / b_{ext}(PM_{10})$  ratio. The black and blue  
 581 traces are the  $FMF_{ext}$  from the SDA analysis of the CRD extinction (black) and nephelometer +  
 582 PSAP extinction (blue). The  $FMF_{ext,CRD}$  values are the same as those of Fig. 1 for the latter half of  
 583 the campaign. Uncertainty ranges are shown as light colored bands. The uncertainty of  $SMF_{ext,sum}$  is  
 584 only slightly wider than the heavy line that was chosen to represent it.



Deleted:

Formatted: Line spacing: single

585

587 The  $FMF_{ext,CRD}$  was determined for  $PM_{2.5}$  while the  $FMF_{ext,sum}$  was determined for  $PM_{10}$ . If a substantial  
588 fraction of the scattering was contributed by particles with diameters  $>2.5 \mu m$ , then the  $FMF_{ext,CRD}$   
589 should be larger than the  $FMF_{ext,sum}$ , as was observed. Kassianov et al. (2012) used measured particle  
590 size distributions from CARES to show that supermicron particles contributed significantly to the total  
591 scattering, consistent with the observation that  $FMF_{ext,CRD} > FMF_{ext,sum}$ . Variability in the difference  
592 between the  $FMF_{ext,CRD}$  and  $FMF_{ext,sum}$  likely reflects variability in the contribution of these larger  
593 particles to the total scattering.

594 The  $FMF_{ext,CRD}$ ,  $FMF_{ext,sum}$  and  $SMF_{ext,sum}$  were similarly determined from the measurements at the T1 site  
595 (Figure 3). For T1, the CRD measurements were made for particles without any intentional size cut  
596 applied, as opposed to the  $PM_{2.5}$  size cut used for the T0 measurements. At this downwind site the  
597  $SMF_{ext,sum}$ ,  $FMF_{ext,CRD}$  and  $FMF_{ext,sum}$  were all very similar, both in terms of the absolute magnitude and  
598 the temporal variability. The  $FMF_{ext,CRD}$  ranged from 0.22 to 0.89, with a mean of  $0.58 \pm 0.16$ . That the  
599  $FMF_{ext,CRD}$  and  $FMF_{ext,sum}$  are very similar in absolute magnitude for T1 but differ at T0 (while still  
600 exhibiting similar temporal variability) is likely related to the application of an intentional size cut for the  
601 CRD measurements at T0 but not at T1. The observations suggest that the T1 CRD without the size cut  
602 samples coarse-mode particles with a similar efficiency as the nephelometer and PSAP having the  $PM_{10}$   
603 size cut.

604 Overall, these results indicate that the use of the spectral deconvolution algorithm on optical data can  
605 robustly provide information on the fine mode fraction of extinction. Moreover, since the  $FMF_{ext}$  results  
606 at T1 are similar for the two types of extinction measurements, it seems that the narrower wavelength  
607 range of the nephelometer (450, 550, 700 nm) and PSAP (470, 522, 660 nm) compared to the CRD  
608 instruments used here is still adequate to define the spectral dependence of extinction for extraction of  
609 the slope and curvature parameters. However, the results demonstrate that the optical method does  
610 not allow for a precise definition of “fine” and “coarse” in terms of a specific, effective size cut that  
611 distinguishes between the two regimes. While the SMF has an explicitly defined size cut ( $PM_{1}$ ), the  
612 effective size cut for the FMF can vary. The effective size cut is dependent on the shapes (i.e. widths,  
613 positions and number of actual modes) of the size distributions in the “fine” and “coarse” size regimes  
614 and the extent of overlap between them, which is dependent on the size range of particles sampled (e.g.  
615  $PM_{2.5}$  versus  $PM_{10}$ ). For remote sensing measurements, the particular size that distinguishes between  
616 the fine and coarse mode therefore likely varies between locations and seasons. Nonetheless, since the  
617 major sources of fine and coarse mode particles are likely to be reasonably distinct in many

Deleted: 3

Deleted: 85

Deleted: 66

Deleted: 19

Deleted: differences observed at both sites highlight the fact

Deleted: there is not

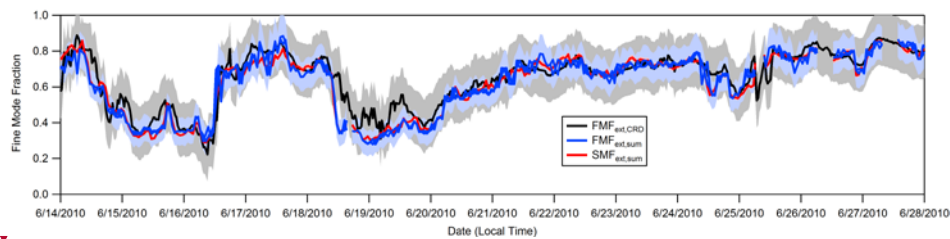
Deleted: in

Deleted: optical method.

627 environments, the  $FMF_{ext,CRD}$  provides a reasonable characterization of the variability in the  
628 contributions of such sources to the total extinction and, in environments where the extinction is  
629 dominated by scattering (i.e. when the SSA is large), to the total scattering as well.

Deleted: can provide a

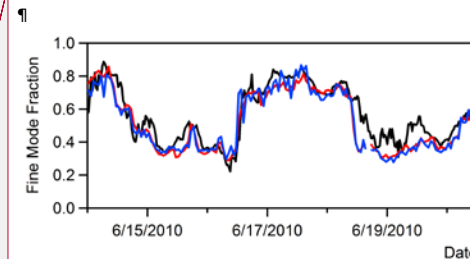
630



631

632 **Figure 3** – the fine mode fraction of extinction (SMF and  $FMF_{ext}$ ) for the latter half of the  
633 campaign at T1. Here, the  $FMF_{ext,CRD}$  is determined for particles sampled without a size cut  
634 applied. Uncertainty ranges are shown as light colored bands.

Deleted: ¶



Formatted: Line spacing: single

635

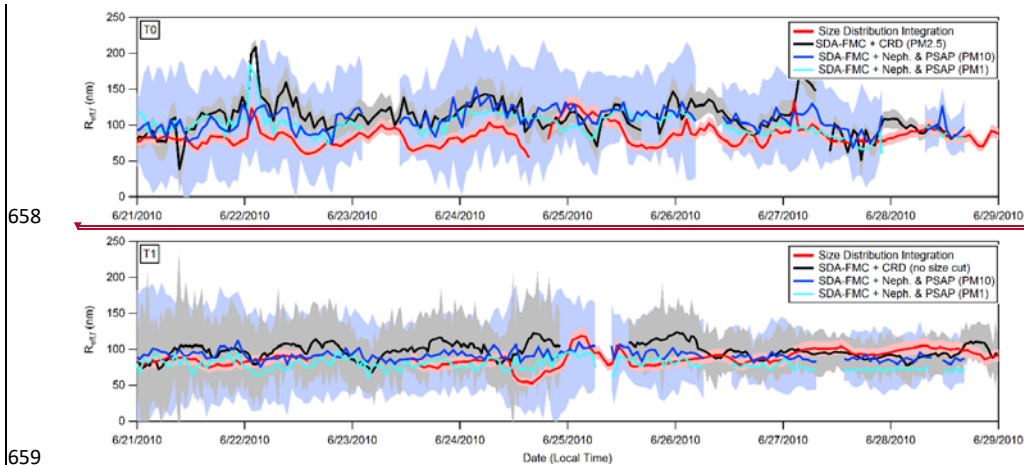
### 636 *Effective fine mode radius product of SDA-FMC*

Formatted: Font: Italic

637 The SDA-FMC analysis also allows for derivation of the fine mode effective radius,  $R_{eff,f}$ , via Eq. 3.  
638 Determination of  $R_{eff,f}$  requires knowledge of the real and imaginary parts of the refractive index. Here,  
639 an average value of  $m_r = 1.5$  is used, based on Atkinson et al. (2015), and absorption is assumed to be  
640 negligible. The latter is a reasonable assumption given the relatively high single scatter albedo values at  
641 the two sites (Cappa et al., 2016), and because assuming the particles to be slightly absorbing has  
642 minimal influence on the results. Temporal variability in  $m_r$  due to variability in particle composition will  
643 contribute to uncertainty in the retrieved  $R_{eff,f}$ . As discussed above, a change in  $m_r$  of 0.13 corresponds  
644 approximately to a shift in  $R_{eff,f}$  by 30%. The actual variability in  $m_r$  is not known for the particles here,  
645 but we expect a shift of 0.13 in  $m_r$  to be a reasonable upper limit on physical grounds.

Deleted: 55

646 Values of  $R_{eff,f}$  are determined using both the CRD-measured  $b_{ext}$  and the  $PM_{10}$   $b_{ext}$  from the  
647 nephelometer + PSAP measurements for both T0 and T1 (Figure 4).  $R_{eff,f}$  values are also determined  
648 from the  $PM_1$  nephelometer + PSAP measurements at both sites. Comparison of the  $R_{eff,f}$  values  
649 between the  $PM_{10}$  and  $PM_1$  measurements provides a test of the robustness of the overall retrieval  
650 method. The  $R_{eff,f}$  from the CRD measurements will be referred to as  $R_{eff,f,CRD}$  and from the  
651 nephelometer + PSAP as  $R_{eff,f,sum}$ . Comparator values of  $R_{eff,f}$  were also calculated from the observed  
652 mobility size distributions using Eqn. 1, and are referred to as  $R_{eff,f,size}$ .



658

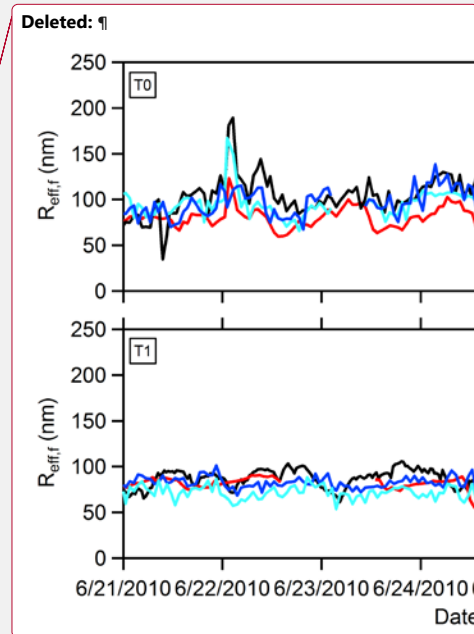
659

660 **Figure 4** – Time series of the effective fine mode radii,  $R_{eff,f}$ , produced by the SDA-FMC analysis of the  
 661 CRD data (black) and the nephelometer + PSAP data (blue) from T0 (top) and T1 (bottom). For the  
 662 nephelometer + PSAP observations, separate results are shown using either the PM<sub>10</sub> (dark blue) or  
 663 PM<sub>1</sub> (light blue) observations. The  $R_{eff,f}$  values determined from the size distribution measurements  
 664 (i.e. from Eqn. 1) are shown in red. Uncertainty ranges are shown as light colored bands for each  
 665 method; for the SDA-FMC the uncertainty range is only shown for PM<sub>10</sub> to avoid clutter, but the  
 666 uncertainty range is similar for PM<sub>1</sub>.

667

668 The SDA-FMC-derived  $R_{eff,f}$  values from the CRD and from the nephelometer + PSAP exhibit reasonably  
 669 good agreement in terms of the absolute values and the temporal variability at both the T0 and T1 sites  
 670 (Table 2, Fig. 4). Notably, there is good agreement between the  $R_{eff,f,sum}$  values obtained from the PM<sub>10</sub>  
 671 and PM<sub>1</sub> measurements. This provides an important validation of the SDA-FMC procedure, since the  
 672 coarse mode contribution to the PM<sub>10</sub> extinction is substantial and highly variable (Figure 2 and Figure  
 673 3).

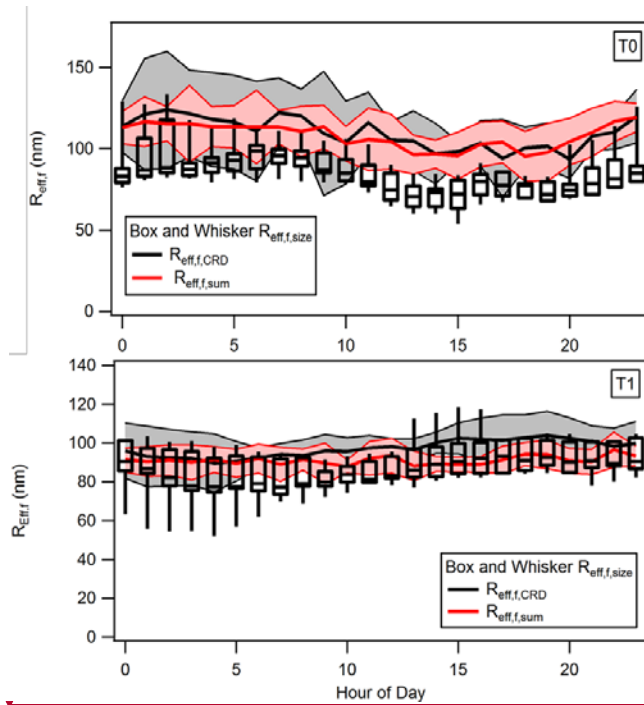
674 At T0, the derived  $R_{eff,f}$  values range from approximately 70 nm to 140 nm (Table 2), with a few short-  
 675 duration periods when  $R_{eff,f}$  is outside this range, reflecting short-duration variability in the particle  
 676 sources. At T1 the derived  $R_{eff,f}$  are generally less variable, ranging from approximately 65 nm to 110 nm,  
 677 with fewer particularly low or high periods. The mean  $R_{eff,f}$  values between the two sites are similar  
 678 (Table 2). At T0, there is a fair degree of temporal coherence of the SDA-FMC results and those obtained  
 679 from integration of the size distributions. The generally good temporal agreement between the  
 680 optically- and size-derived  $R_{eff,f}$  values are even observed during periods where the changes in radius



683 happened rapidly, for example near midnight between June 21-22. On that night there is some evidence  
684 that paving operations near the T0 site produced a strong local source of asphalt particles in the coarse  
685 mode with a long tail into the sub-micron regime (Zaveri et al., 2012; Cappa et al., 2016). This short-  
686 duration source of large particles pushed the  $R_{\text{eff},f}$  temporarily towards larger values. (The  $R_{\text{eff},f}$  changes  
687 from the nephelometer + PSAP at this time were smaller than from the CRD or size distribution  
688 observations. Most likely this reflects the alternating 6-min sampling of the nephelometer and the very  
689 short duration of the event leading to discrepancies in the 1 h average.)

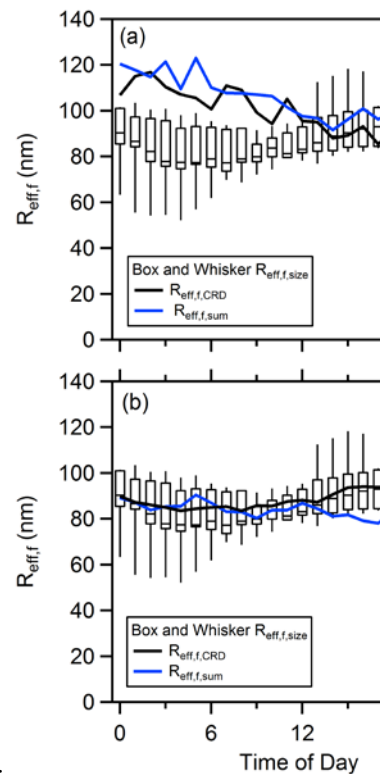
690 Despite the generally good correspondence between  $R_{\text{eff},f,\text{size}}$  and the optically derived values, the  
691  $R_{\text{eff},f,\text{size}}$  values were often (but not always) smaller (Table 2). This is most clearly seen when comparing  
692 the average diurnal profiles of the  $R_{\text{eff},f}$  values from the different methods, as shown in Figure 5. All  
693 three  $R_{\text{eff},f}$  estimates exhibit similar diurnal behavior at T0, even though the  $R_{\text{eff},f}$  from the SDA-FMC  
694 method are larger than  $R_{\text{eff},f,\text{size}}$ . The diurnal variability in the  $R_{\text{eff},f}$  is more pronounced at T0 than at T1.  
695 The diurnal trend in the effective radius of the fine mode at T0 from all methods exhibits a minimum at  
696 around mid-day and then an increase to a maximum right near daybreak. Particle number and sizes at  
697 both sites were influenced by frequent regional new particle formation and growth events during CARES  
698 (see Figure S2). The events tended to start in the morning with a sharp increase of 10 - 20 nm particles  
699 followed by growth of these particles to 50 – 100 nm in the afternoon as discussed in Setyan et al.  
700 (2014). The next day the cycle repeats (on average) with the introduction of the new small particles  
701 which has the effect of decreasing the average particle radius (Setyan et al., 2014). Although observed at  
702 both sites, the new particle formation events had a greater impact on the size distributions at T0,  
703 especially in terms of surface area-weighted size distributions (Figure S3) that determine  $R_{\text{eff},f}$ . In part,  
704 this is likely because of continued growth of the new particle mode as it transits from T0 to T1. In  
705 addition, for T0 there is a notable mode in the surface-area weighted distribution at ~1 micron that is  
706 most evident in the early morning (Figure S3). This mode has little influence on the  $R_{\text{eff},f}$  values  
707 determined from the size distributions, but contributes to the higher optically determined  $R_{\text{eff},f}$  values in  
708 the early morning for T0. This mode is much less prevalent at the T1 site, and thus there is better  
709 correspondence between the size-distribution and optical methods.

710



711  
 712 **Figure 5** – The diurnal dependence of  $R_{eff,f}$  for the period shown in Fig. 4 for the (top) T0 and  
 713 (bottom) T1 sites. The box and whisker plot (bottom and top of box are 5% and 95% of data  
 714 range, bar is mean, and whiskers extend to full range) shows the results from the direct size  
 715 distribution measurement ( $R_{eff,f,size}$ ). The thick lines show the mean diurnal dependence of the  
 716 optically derived  $R_{eff,f}$ , using the CRD (black) and nephelometer + PSAP (red) measurements. The  
 717 light colored bands show the  $\pm 1\sigma$  standard deviation based on the measurement variability over  
 718 the averaging period.

719  
 720 One possible explanation for the differences between the optically and size-derived  $R_{eff,f}$ , in particular at  
 721 T0, may be inaccurate specification of the refractive index. Temporal variations in or an overall offset of  
 722 the real refractive index used here from the true value would lead to errors in the optically derived  $R_{eff,f}$ .  
 723 The refractive index is used to convert the derived van de Hulst parameter to  $R_{eff,f}$  (Eqn. 3). Given the  
 724 form of the relationship, an absolute error in the real RI of 0.1—likely an upper limit—corresponds to an  
 725 error in the derived  $R_{eff,f}$  of 20%, with larger values of the real RI leading to smaller derived  $R_{eff,f}$ . The  
 726 imaginary component was assumed zero. The effective imaginary RI is likely  $\leq 0.01$ , given the range of  
 727 single scatter albedo values observed (Cappa et al., 2016). Thus, the assumption of zero for the



Deleted:  
 Deleted: a  
 Deleted: b  
 Deleted: ), while the  
 Deleted: blue) measurements.



795 determined from near-coincident measurement of extinction by  $PM_{10}$  and  $PM_{10}$ , provides insights into  
796 the effective  $FMF_{ext}$  split size. For one of the sites considered here the split point size is around  $1 \mu m$   
797 while for the other it is somewhat larger than  $1 \mu m$  and perhaps more variable. In many environments,  
798 variability in aerosol properties on short (<10 min) timescales is relatively minimal. In such cases, a single  
799 instrument can be used to sequentially sample  $PM_{10}$  and  $PM_{10}$ , allowing for *in situ* measurement of both  
800 the  $FMF_{ext}$  and  $SMF_{ext}$ . However, remote sensing measurements characterize only the  $FMF_{ext}$ , (or at  
801 best, an optically influenced size cut as is done in the AERONET retrievals of Dubovik & King, 2000).  
802 Thus, further consideration of *in situ* measurement results, such as those investigated in this study, can  
803 provide insights into the interpretation of the  $FMF_{ext}$  determined from remote sensing in different  
804 environments.

805 The SDA-FMC approach also allows for determination of the effective fine mode radius. The  $R_{eff,f}$   
806 characterizes the surface-area weighted size of the particles within the fine mode distribution. The  
807 similarity of the results in Figure 4 for application of the SDA-FMC to both size-selected and non-size-  
808 selected aerosol as well as the comparison with results derived from the PSD measurements verify that  
809 “whole air” measurements (i.e., no imposed size-selection) can provide reliable fine mode radii at least  
810 for large  $FMF$  values.

## 811 **Acknowledgements**

812 This work was supported by the Atmospheric System Research (ASR) program sponsored by the US  
813 Department of Energy (DOE), Office of Biological and Environmental Research (OBER), including Grant  
814 No. DE-SC0008937. Funding for data collection was provided by the US DOE’s Atmospheric Radiation  
815 Measurement (ARM) Program. All data used in this study are available from the ARM data archive at:  
816 <http://www.arm.gov/campaigns/aaf2009carbonaerosol>. The views expressed in this document are  
817 solely those of the authors and the funding agencies do not endorse any products or commercial  
818 services mentioned in this publication.

819 **Appendix A – Glossary of Symbols and Acronyms used**

820	$\hat{\lambda}$	Ångström exponent (from wavelength pair)
821	$\alpha$	Spectral derivative of optical property
822	$\alpha'$	Curvature (second derivative of optical property in log-log space)
823	$\alpha_r$ or $\alpha'_r$	Fine mode version of properties (also coarse mode properties $\alpha_c$ )
824	AOD	Aerosol optical depth
825	$b_{\text{ext}}, b_{\text{scat}}, b_{\text{abs}}$	Optical coefficient for extinction, scattering, absorption (inverse length units)
826	CRD	Cavity ring down
827	$R_{\text{eff},s}$	Effective radius for fine mode
828	FMF (aka $\eta$ )	Fine mode fraction of an optical property, usually extinction
829	SMF	Sub-micron fraction (particle mode with radius or diameter smaller than 1 $\mu\text{m}$ )
830	<del><math>Q_{\text{eff},f}</math></del>	<b>Effective</b> fine mode van de Hulst parameter (product of refractive index and
831		effective radius)
832	SDA	Spectral Deconvolution Algorithm
833	FMC	Fine Mode Curvature approach
834	$\text{PM}_1$	Particulate matter with diameter (or radius) smaller than 1 $\mu\text{m}$ (also $\text{PM}_{2.5}$ , $\text{PM}_{10}$ )
835	PSAP	Particle soot absorption photometer instrument
836		

Deleted:  $\rho_f$  . . .

Formatted: Indent: Left: 0", Hanging: 1"

838 **References:**

- 839 Anderson, T. L., Charlson, R. J., Bellouin, N., Boucher, O., Chin, M., Christopher, S. A., Haywood, J.,  
840 Kaufman, Y. J., Kinne, S., Ogren, J. A., Remer, L. A., Takemura, T., Tanre, D., Torres, O., Treppe, C. R.,  
841 Wielicki, B. A., Winker, D. M., and Yu, H. B.: An "A-Train" strategy for quantifying direct climate forcing  
842 by anthropogenic aerosols, *B. Am. Meteorol. Soc.*, 86, 1795-1805, doi:10.1175/Bams-86-12-1795, 2005.
- 843 [Anderson, T. L. and Ogren, J. A.: Determining Aerosol Radiative Properties Using the TSI 3563 Integrating](#)  
844 [Nephelometer, \*Aerosol Sci. Technol.\*, 29, 57-69, doi:10.1080/02786829808965551, 1998.](#)
- 845 Andrews, E., Sheridan, P. J., Ogren, J. A., and Ferrare, R.: In situ aerosol profiles over the Southern Great  
846 Plains cloud and radiation test bed site: 1. Aerosol optical properties, *J. Geophys. Res.-Atmos.*, 109,  
847 D06208, doi:10.1029/2003jd004025, 2004.
- 848 Ångström, A.: On the atmospheric transmission of sun radiation and on dust in the air, *Geografika Ann.*,  
849 11, 156-166, doi:10.2307/519399, 1929.
- 850 Atkinson, D. B., Massoli, P., O'Neill, N. T., Quinn, P. K., Brooks, S. D., and Lefer, B.: Comparison of in situ  
851 and columnar aerosol spectral measurements during TexAQS-GoMACCS 2006: testing parameterizations  
852 for estimating aerosol fine mode properties, *Atmos. Chem. Phys.*, 10, 51-61, doi:10.5194/acp-10-51-  
853 2010, 2010.
- 854 Atkinson, D. B., Radney, J. G., Lum, J., Kolesar, K. R., Cziczo, D. J., Pekour, M. S., Zhang, Q., Setyan, A.,  
855 Zelenyuk, A., and Cappa, C. D.: Aerosol optical hygroscopicity measurements during the 2010 CARES  
856 campaign, *Atmos. Chem. Phys.*, 15, 4045-4061, doi:10.5194/acp-15-4045-2015, 2015.
- 857 Baibakov, K., O'Neill, N. T., Ivanescu, L., Duck, T. J., Perro, C., Herber, A., Schulz, K. H., and Schrems, O.:  
858 Synchronous polar winter starphotometry and lidar measurements at a High Arctic station, *Atmos.*  
859 *Meas. Techniq.*, 8, 3789-3809, doi:10.5194/amt-8-3789-2015, 2015.
- 860 Bokoye, A. I., Royer, A., O'Neill, N. T., Cliche, P., Fedosejevs, G., Teillet, P. M., and McArthur, L. J. B.:  
861 Characterization of atmospheric aerosols across Canada from a ground-based sunphotometer network:  
862 AEROCAN, *Atmosphere-Ocean*, 39, 429-456, doi:10.1080/07055900.2001.9649687, 2001.
- 863 Bond, T. C., Zarzycki, C., Flanner, M. G., and Koch, D. M.: Quantifying immediate radiative forcing by  
864 black carbon and organic matter with the Specific Forcing Pulse, *Atmos. Chem. Phys.*, 11, 1505-1525,  
865 doi:10.5194/acp-11-1505-2011, 2011.
- 866 Brown, S. S.: Absorption Spectroscopy in High-Finesse Cavities for Atmospheric Studies, *Chemical*  
867 *Reviews*, 103, 5219-5238, doi:10.1021/cr020645c, 2003.
- 868 Cappa, C. D., Kolesar, K. R., Zhang, X. L., Atkinson, D. B., Pekour, M. S., Zaveri, R. A., Zelenyuk, A., and  
869 Zhang, Q.: Understanding the optical properties of ambient sub- and supermicron particulate matter:  
870 results from the CARES 2010 field study in northern California, *Atmos. Chem. Phys.*, 16, 6511-6535,  
871 doi:10.5194/acp-16-6511-2016, 2016.
- 872 Charlson, R. J., Valero, F. P. J., and Seinfeld, J. H.: In search of balance, *Science*, 308, 806-807,  
873 doi:10.1126/science.1108162, 2005.

874 Clarke, A. and Kapustin, V.: Hemispheric Aerosol Vertical Profiles: Anthropogenic Impacts on Optical  
875 Depth and Cloud Nuclei, *Science*, 329, 1488-1492, doi:10.1126/science.1188838, 2010.

876 Coen, M. C., Andrews, E., Asmi, A., Baltensperger, U., Bukowiecki, N., Day, D., Fiebig, M., Fjaeraa, A. M.,  
877 Flentje, H., Hyvarinen, A., Jefferson, A., Jennings, S. G., Kouvarakis, G., Lihavainen, H., Myhre, C. L.,  
878 Malm, W. C., Mihapopoulos, N., Molenaar, J. V., O'Dowd, C., Ogren, J. A., Schichtel, B. A., Sheridan, P.,  
879 Virkkula, A., Weingartner, E., Weller, R., and Laj, P.: Aerosol decadal trends - Part 1: In-situ optical  
880 measurements at GAW and IMPROVE stations, *Atmos. Chem. Phys.*, 13, 869-894, doi:10.5194/acp-13-  
881 869-2013, 2013.

882 Doran, J. C., Barnard, J. C., Arnott, W. P., Cary, R., Coulter, R., Fast, J. D., Kassianov, E. I., Kleinman, L.,  
883 Laulainen, N. S., Martin, T., Paredes-Miranda, G., Pekour, M. S., Shaw, W. J., Smith, D. F., Springston, S.  
884 R., and Yu, X. Y.: The T1-T2 study: evolution of aerosol properties downwind of Mexico City, *Atmos.*  
885 *Chem. Phys.*, 7, 1585-1598, doi:10.5194/acp-7-1585-2007, 2007.

886 Dubovik, O. and King, M. D.: A flexible inversion algorithm for retrieval of aerosol optical properties from  
887 Sun and sky radiance measurements, *J. Geophys. Res.-Atmos.*, 105, 20673-20696,  
888 doi:10.1029/2000jd900282, 2000.

889 Eck, T. F., Holben, B. N., Reid, J. S., Sinyuk, A., Dubovik, O., Smirnov, A., Giles, D., O'Neill, N. T., Tsay, S. C.,  
890 Ji, Q., Al Mandoos, A., Khan, M. R., Reid, E. A., Schafer, J. S., Sorokine, M., Newcomb, W., and Slutsker, I.:  
891 Spatial and temporal variability of column-integrated aerosol optical properties in the southern Arabian  
892 Gulf and United Arab Emirates in summer, *J. Geophys. Res.-Atmos.*, 113, D01204,  
893 doi:10.1029/2007jd008944, 2008.

894 Fast, J. D., Gustafson, W. I., Berg, L. K., Shaw, W. J., Pekour, M., Shrivastava, M., Barnard, J. C., Ferrare, R.  
895 A., Hostetler, C. A., Hair, J. A., Erickson, M., Jobson, B. T., Flowers, B., Dubey, M. K., Springston, S., Pierce,  
896 R. B., Dolislager, L., Pederson, J., and Zaveri, R. A.: Transport and mixing patterns over Central California  
897 during the carbonaceous aerosol and radiative effects study (CARES), *Atmos. Chem. Phys.*, 12, 1759-  
898 1783, doi:10.5194/acp-12-1759-2012, 2012.

899 George, I. J. and Abbatt, J. P. D.: Heterogeneous oxidation of atmospheric aerosol particles by gas-phase  
900 radicals, *Nature Chemistry*, 2, 713-722, doi:10.1038/nchem.806, 2010.

901 Hamill, P., Giordano, M., Ward, C., Giles, D., and Holben, B.: An AERONET-based aerosol classification  
902 using the Mahalanobis distance, *Atmos. Environ.*, 140, 213-233, doi:10.1016/j.atmosenv.2016.06.002,  
903 2016.

904 Hansen, J. E. and Travis, L. D.: Light-Scattering in Planetary Atmospheres, *Space Sci. Rev.*, 16, 527-610,  
905 doi:10.1007/Bf00168069, 1974.

906 Holben, B. N., Eck, T. F., Slutsker, I., Tanre, D., Buis, J. P., Setzer, A., Vermote, E., Reagan, J. A., Kaufman,  
907 Y. J., Nakajima, T., Lavenu, F., Jankowiak, I., and Smirnov, A.: AERONET - A federated instrument network  
908 and data archive for aerosol characterization, *Remote Sens. Environ.*, 66, 1-16, doi:10.1016/S0034-  
909 4257(98)00031-5, 1998.

910 IPCC: Climate Change 2013: The Physical Science Basis. Contribution of Working Group I to the Fifth  
911 Assessment Report of the Intergovernmental Panel on Climate Change, Cambridge University Press,  
912 Cambridge, United Kingdom and New York, NY, USA, 2013.

913 Kaku, K. C., Reid, J. S., O'Neill, N. T., Quinn, P. K., Coffman, D. J., and Eck, T. F.: Verification and  
914 application of the extended spectral deconvolution algorithm (SDA plus ) methodology to estimate  
915 aerosol fine and coarse mode extinction coefficients in the marine boundary layer, *Atmos. Meas.*  
916 *Techniq.*, 7, 3399-3412, doi:10.5194/amt-7-3399-2014, 2014.

917 Lack, D. A. and Cappa, C. D.: Impact of brown and clear carbon on light absorption enhancement, single  
918 scatter albedo and absorption wavelength dependence of black carbon, *Atmos. Chem. Phys.*, 10, 4207-  
919 4220, doi:10.5194/acp-10-4207-2010, 2010.

920 Lack, D. A., Richardson, M. S., Law, D., Langridge, J. M., Cappa, C. D., McLaughlin, R. J., and Murphy, D.  
921 M.: Aircraft Instrument for Comprehensive Characterization of Aerosol Optical Properties, Part 2: Black  
922 and Brown Carbon Absorption and Absorption Enhancement Measured with Photo Acoustic  
923 Spectroscopy, *Aerosol Science and Technology*, 46, 555-568, doi:10.1080/02786826.2011.645955, 2012.

924 Langridge, J. M., Richardson, M. S., Lack, D., Law, D., and Murphy, D. M.: Aircraft Instrument for  
925 Comprehensive Characterization of Aerosol Optical Properties, Part I: Wavelength-Dependent Optical  
926 Extinction and Its Relative Humidity Dependence Measured Using Cavity Ringdown Spectroscopy,  
927 *Aerosol Science and Technology*, 45, 1305-1318, doi:10.1080/02786826.2011.592745, 2011.

928 Massoli, P., Bates, T. S., Quinn, P. K., Lack, D. A., Baynard, T., Lerner, B. M., Tucker, S. C., Brioude, J.,  
929 Stohl, A., and Williams, E. J.: Aerosol optical and hygroscopic properties during TexAQs-GoMACCS 2006  
930 and their impact on aerosol direct radiative forcing, *J. Geophys. Res.-Atmos.*, 114, D00f07,  
931 doi:10.1029/2008jd011604, 2009.

932 Moosmuller, H., Chakrabarty, R. K., and Arnott, W. P.: Aerosol light absorption and its measurement: A  
933 review, *J Quant. Spec. Rad. Trans.*, 110, 844-878, doi:10.1016/j.jqsrt.2009.02.035, 2009.

934 O'Neill, N. T., Eck, T. F., Holben, B. N., Smirnov, A., Dubovik, O., and Royer, A.: Bimodal size distribution  
935 influences on the variation of Angstrom derivatives in spectral and optical depth space, *J. Geophys. Res.-*  
936 *Atmos.*, 106, 9787-9806, doi:10.1029/2000jd900245, 2001.

937 O'Neill, N. T., Eck, T. F., Reid, J. S., Smirnov, A., and Pancrati, O.: Coarse mode optical information  
938 retrievable using ultraviolet to short-wave infrared sun photometry: Application to United Arab Emirates  
939 unified aerosol experiment data, *J. Geophys. Res.-Atmos.*, 113, D05212, doi:10.1029/2007jd009052,  
940 2008a.

941 O'Neill, N. T., Eck, T. F., Smirnov, A., Holben, B. N., and Thulasiraman, S.: Spectral discrimination of  
942 coarse and fine mode optical depth, *J. Geophys. Res.-Atmos.*, 108, 4559, doi:10.1029/2002jd002975,  
943 2003.

944 O'Neill, N. T., Thulasiraman, S., Eck, T. F., and Reid, J. S.: [Robust optical features of fine mode size](#)  
945 [distributions: Application](#) to the [Quebec smoke event of 2002](#), *J. Geophys. Res.-Atmos.*, 110, D11207,  
946 doi:10.1029/2004jd005157, 2005.

947 O'Neill, N. T., Thulasiraman, S., Eck, T. F., and Reid, J. S.: [Correction to the effective radius expression in](#)  
948 [O'Neill et al. \(2005\)](#), *J. Geophys. Res.-Atmos.*, 113, D24203, doi:10.1029/2008JD011334, 2008b.

- Deleted:** Correction
- Deleted:** effective radius expression in O'Neill et al. (2005),
- Deleted:** Atmos., 113, D24203
- Deleted:** 2008JD011334, 2008b
- Deleted:** Robust optical features of fine mode size distributions: Application
- Deleted:** Quebec smoke event of 2002,
- Deleted:** Atmos., 110, D11207
- Deleted:** 2004jd005157, 2005

958 [Ogren, J. A.: Comment on "Calibration and Intercomparison of Filter-Based Measurements of Visible](#)  
959 [Light Absorption by Aerosols", Aerosol Sci. Technol., 44, 589-591, doi:10.1080/02786826.2010.482111,](#)  
960 [2010.](#)

961 Radney, J. G., Bazargan, M. H., Wright, M. E., and Atkinson, D. B.: Laboratory Validation of Aerosol  
962 Extinction Coefficient Measurements by a Field-Deployable Pulsed Cavity Ring-Down Transmissometer,  
963 *Aerosol Science and Technology*, 43, 71-80, doi:10.1080/02786820802482536, 2009.

964 Saha, A., O'Neill, N. T., Eloranta, E., Stone, R. S., Eck, T. F., Zidane, S., Daou, D., Lupu, A., Lesins, G.,  
965 Shiobara, M., and McArthur, L. J. B.: Pan-Arctic sunphotometry during the ARCTAS-A campaign of April  
966 2008, *Geophys. Res. Lett.*, 37, L05803, doi:10.1029/2009gl041375, 2010.

967 Setyan, A., Song, C., Merkel, M., Knighton, W. B., Onasch, T. B., Canagaratna, M. R., Worsnop, D. R.,  
968 Wiedensohler, A., Shilling, J. E., and Zhang, Q.: Chemistry of new particle growth in mixed urban and  
969 biogenic emissions - insights from CARES, *Atmos. Chem. Phys.*, 14, 6477-6494, doi:10.5194/acp-14-6477-  
970 2014, 2014.

971 Setyan, A., Zhang, Q., Merkel, M., Knighton, W. B., Sun, Y., Song, C., Shilling, J. E., Onasch, T. B., Herndon,  
972 S. C., Worsnop, D. R., Fast, J. D., Zaveri, R. A., Berg, L. K., Wiedensohler, A., Flowers, B. A., Dubey, M. K.,  
973 and Subramanian, R.: Characterization of submicron particles influenced by mixed biogenic and  
974 anthropogenic emissions using high-resolution aerosol mass spectrometry: results from CARES, *Atmos.*  
975 *Chem. Phys.*, 12, 8131-8156, doi:10.5194/acp-12-8131-2012, 2012.

976 Smith, J. D. and Atkinson, D. B.: A portable pulsed cavity ring-down transmissometer for measurement  
977 of the optical extinction of the atmospheric aerosol, *Analyst*, 126, 1216-1220, doi:10.1039/B101491,  
978 2001.

979 [Wiedensohler, A., Birmili, W., Nowak, A., Sonntag, A., Weinhold, K., Merkel, M., Wehner, B., Tuch, T.,](#)  
980 [Pfeifer, S., Fiebig, M., Fjåraa, A. M., Asmi, E., Sellegri, K., Depuy, R., Venzac, H., Villani, P., Laj, P., Aalto,](#)  
981 [P., Ogren, J. A., Swietlicki, E., Williams, P., Roldin, P., Quincey, P., Hüglin, C., Fierz-Schmidhauser, R.,](#)  
982 [Gysel, M., Weingartner, E., Riccobono, F., Santos, S., Gröning, C., Faloon, K., Beddows, D., Harrison, R.,](#)  
983 [Monahan, C., Jennings, S. G., O'Dowd, C. D., Marinoni, A., Horn, H. G., Keck, L., Jiang, J., Scheckman, J.,](#)  
984 [McMurry, P. H., Deng, Z., Zhao, C. S., Moerman, M., Henzing, B., de Leeuw, G., Löschau, G., and Bastian,](#)  
985 [S.: Mobility particle size spectrometers: harmonization of technical standards and data structure to](#)  
986 [facilitate high quality long-term observations of atmospheric particle number size distributions, Atmos.](#)  
987 [Meas. Tech., 5, 657-685, doi:10.5194/amt-5-657-2012, 2012.](#)

988 Zaveri, R. A., Shaw, W. J., Cziczo, D. J., Schmid, B., Ferrare, R. A., Alexander, M. L., Alexandrov, M.,  
989 Alvarez, R. J., Arnott, W. P., Atkinson, D. B., Baidar, S., Banta, R. M., Barnard, J. C., Beranek, J., Berg, L. K.,  
990 Brechtel, F., Brewer, W. A., Cahill, J. F., Cairns, B., Cappa, C. D., Chand, D., China, S., Comstock, J. M.,  
991 Dubey, M. K., Easter, R. C., Erickson, M. H., Fast, J. D., Floerchinger, C., Flowers, B. A., Fortner, E.,  
992 Gaffney, J. S., Gilles, M. K., Gorkowski, K., Gustafson, W. I., Gyawali, M., Hair, J., Hardesty, R. M.,  
993 Harworth, J. W., Herndon, S., Hiranuma, N., Hostetler, C., Hubbe, J. M., Jayne, J. T., Jeong, H., Jobson, B.  
994 T., Kassianov, E. I., Kleinman, L. I., Kluzek, C., Knighton, B., Kolesar, K. R., Kuang, C., Kubatova, A.,  
995 Langford, A. O., Laskin, A., Laulainen, N., Marchbanks, R. D., Mazzoleni, C., Mei, F., Moffet, R. C., Nelson,  
996 D., Obland, M. D., Oetjen, H., Onasch, T. B., Ortega, I., Ottaviani, M., Pekour, M., Prather, K. A., Radney,  
997 J. G., Rogers, R. R., Sandberg, S. P., Sedlacek, A., Senff, C. J., Senum, G., Setyan, A., Shilling, J. E.,  
998 Shrivastava, M., Song, C., Springston, S. R., Subramanian, R., Suski, K., Tomlinson, J., Volkamer, R.,  
999 Wallace, H. W., Wang, J., Weickmann, A. M., Worsnop, D. R., Yu, X. Y., Zelenyuk, A., and Zhang, Q.:

1000 Overview of the 2010 Carbonaceous Aerosols and Radiative Effects Study (CARES), Atmos. Chem. Phys.,  
1001 12, 7647-7687, doi:10.5194/acp-12-7647-2012, 2012.

1002

1003

1 **Supplemental Information for “Using Spectral Methods to Obtain Particle Size**  
2 **Information from Optical Data: Applications to Measurements from CARES**  
3 **2010”**

4 Dean B. Atkinson<sup>1</sup>, Mikhail Pekour<sup>2</sup>, Duli Chand<sup>2</sup>, James G. Radney<sup>1,\*\*\*</sup>, Katheryn R. Kolesar<sup>5,\*</sup>, Qi Zhang<sup>3</sup>,  
5 Ari Setyan<sup>3,\*\*</sup>, Norman T. O’Neill<sup>4</sup>, Christopher D. Cappa<sup>5</sup>

6 [1] [Department of Chemistry, Portland State University, Portland, OR, USA, 97207]

7 [2] [Pacific Northwest National Laboratory, Richland, WA, USA, 99352]

8 [3] [Department of Environmental Toxicology, University of California, Davis, CA, USA, 95616]

9 [4] [Centre d’Applications et de Recherches en Télédétection, Université de Sherbrooke, Sherbrooke,  
10 Canada]

11 [5] [Department of Civil and Environmental Engineering, University of California, Davis, CA, USA, 95616]

12 \* Now at: Air Sciences, Inc., Portland, OR, 97214, USA

13 \*\* Now at: Empa, Swiss Federal Laboratories for Materials Science and Technology, 8600 Dübendorf,  
14 Switzerland

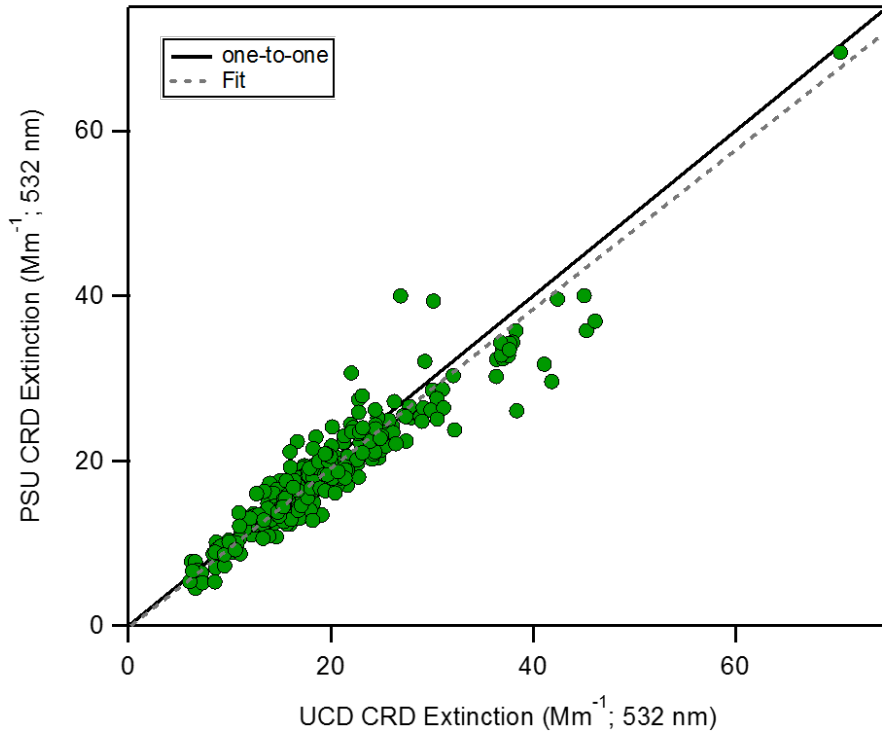
15 \*\*\* Now at: Material Measurement Laboratory, National Institute of Standards and Technology,  
16 Gaithersburg, Maryland, 20899, USA

17 Correspondence to: D. B. Atkinson ([atkinsond@pdx.edu](mailto:atkinsond@pdx.edu))

18

19

20



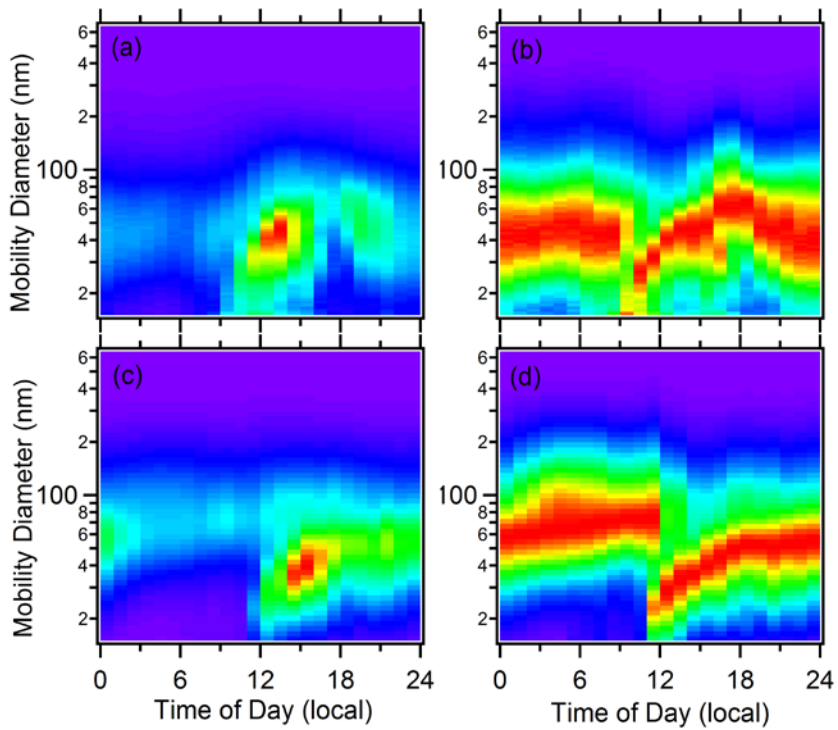
21

22 **Figure S1.** Scatterplot of the visible (532 nm) extinction measurements from the two  
23 CRD instruments used at T0. The solid line in the figure is the 1:1 line while the dashed is  
24 the result of an **orthogonal distance regression** that produced a slope of **0.96** and a  
25 statistically insignificant intercept. Units on both axes are  $Mm^{-1}$ .

26

**Deleted:** linear regression

**Deleted:** 87



29

30 **Figure S2.** Observed diurnal variability in the number-weighted mobility size distribution  
 31 ( $dN/d\log D_p$ ) for (a,b) T0 and (c,d) T1. The color corresponds to particle concentration. (a,c) The  
 32 unnormalized data, with the red indicating the period with the highest concentration. (b,d) The  
 33 size distribution where each hour average is normalized to the maximum concentration during  
 34 that hour. The appearance of a mode associated with new particle formation and growth  
 35 starting at 8 am at T0 and at 11 am at T1 is evident. Data were averaged for June 21-29, 2010.

36

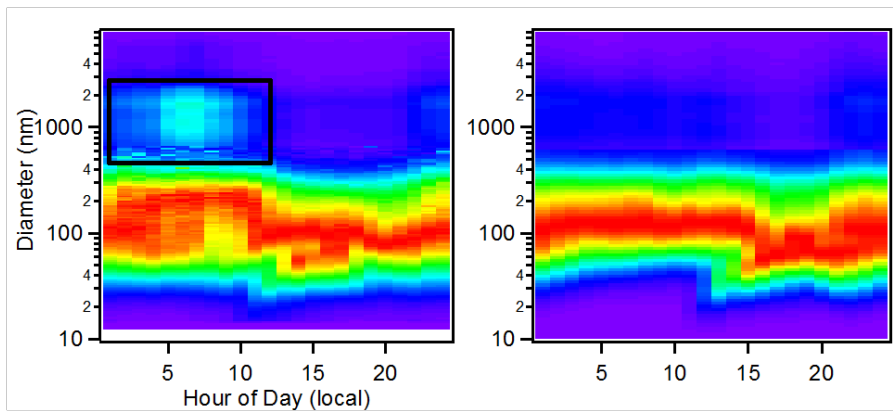


**Figure S3.** Observed diurnal variation for (left) the T0 site and (right) the T1 site for the surface-area weighted size distribution. Distributions have been normalized to the maximum surface area concentration for each hour of the day. The black box shown for T0 highlights the presence of a mode near 1 micron.

37  
38  
39  
40  
41  
42  
43